A Comprehensive Review on Mechanical Amplifier Structures in Piezoelectric Energy Harvesters

Su Xian Long[a], Shin Yee Khoo[a,b,c]*, Zhi Chao Ong[a,b,c], Ming Foong Soong[a], Yu-Hsi Huang[d], Nithiyanandam Prasath[e], and Siamak Noroozi[f]

[a]*Department of Mechanical Engineering, Faculty of Engineering, Universiti Malaya, 50603 Kuala Lumpur, Malaysia.*

[b]*Advanced Shock and Vibration Research Group, Applied Vibration Laboratory, Block R, Faculty of Engineering, Universiti Malaya, 50603, Kuala Lumpur, Malaysia.*

[c]*Centre of Research Industry 4.0 (CRI 4.0), Faculty of Engineering, Universiti Malaya, 50603 Kuala Lumpur, Malaysia.*

[d]*Department of Mechanical Engineering, National Taiwan University, Taipei 10617, Taiwan (R.O.C.).*

[e]*Department of Networking and Communications, Kattankulathur Campus, SRM Institute of Science and Technology, Kanchipuram, India.*

[f]*School of Design, Engineering & Computing, Bournemouth University, Poole, Dorset, BH12 5BB, UK.*

*E-mail: khooshinyee@um.edu.my; mikeson.khoo@yahoo.com

A Comprehensive Review on Mechanical Amplifier Structures in Piezoelectric Energy Harvesters

This paper presents a comprehensive review of structural optimization for the piezoelectric energy harvesters by summarizing the characteristics, working principles, advantages, disadvantages, performance, evaluation factors, and potential applications of each amplifier structure. This includes the cantilever, flexure structure, combined structure, multistage structure, and derivative designs such as compound and hinge designs. Examples and optimization method of structural design which utilizes the compressive mode, 33-mode configuration, and stacking design of piezoelectric material is provided. The power output, amplification ratio, and the applied mechanism theory of each structure are then compared and discussed to ease the benchmarking process for future research.

Keywords: Cantilever; Cymbal; Flexcompressive; Flextensional; Multistage; Rhombus.

Running Head: Review of Amplifier Structure in PEH

Highlights:

- Mechanical amplifier frames relevant to piezoelectric transducer are reviewed.
- Summarized previous work on design characteristics, applications, pros, and cons.
- Figure of merit with power density and amplification factor is presented.
- Design trends and guidance are provided for future research.

1. Introduction

In recent years, the piezoelectric transducer has attracted much attention in several applications such as sensing, energy harvesting, and actuation. Harvesting electrical energy from mechanical vibration has become the main focus of many researchers in developing a sustainable piezoelectric energy harvester (PEH), especially for Wireless Sensor Network (WSN) [1, 2]. Piezoelectric transducers are widely used in the field of energy harvesting since it has higher capacitance, higher voltage output, more effective in low frequencies, and more flexible to be integrated into a system than electromagnetic and electrostatic [3, 4] since it has the amenability to miniaturization. The development of a high-efficiency PEH is essential to provide sufficient power for electronic devices which are getting smaller physically as technology advances such as the self-powered Internet of Things (IoT) devices or WSN in remote places [5, 6].

To improve the performance of the transducer, various approaches can be employed, including structural design with force amplification effects such as on the geometry, configuration, or parameter optimization [7, 8]. The mechanical amplifier structure (MAS), which is also known as the amplification frame, is a structural frame design that enlarges the input loading to a much higher output mechanical physical quantities such as displacement and force. With the amplified force or displacement acting on the piezoelectric material (piezo), the power output of the PEH can be enhanced [9]. For example, the cantilever is a type of MAS that can amplify low displacement into higher displacement by adjusting its natural frequency to match the excitation frequency. This resonance condition allows the deflection and deformation of the piezo to be effectively amplified. On the other hand, the flexure structure is developed to amplify the loading force into higher amplitude, which compresses or extends the piezo under larger stress, leading to higher power output in a PEH [10].

The most commonly used piezo in PEH is the ceramic type, e.g. Lead Zirconate Titanate (PZT) and environmentally friendly lead-free material, e.g. Sodium Potassium Niobate (KNN) & Barium titanate (BT). Other types of piezo include polymer type, e.g. Polyvinylidene Fluoride (PVDF) [11, 12], nanomaterial type, e.g. Zinc Oxide (ZnO) nanorods & nanowires [13], and composite type, e.g. micro fiber composite (MFC) & PZT–polymer composite, which is the compound of PZT and PVDF with adequate thermal and mechanical properties [1]. Since PZT has relatively high piezoelectric coefficients and comparatively higher efficiency, thus it is the main focus piezo in this review [7].

1.1 Piezoelectric Effects

A direct piezoelectric effect is described as an electric field produced by applying mechanical stress on the piezoelectric, which is the fundamental used in the PEH. Conversely, the piezoelectric will deform when there is an external voltage applied on it which is named as the converse or inverse piezoelectric effect and applied in the actuator [8]. The general constitutive of direct and converse effects can be calculated as below [14].

Direct effect: $$D_m = d_{mi}T_i + \varepsilon^T_{mk}E_k \quad (1)$$

Converse effect: $$S_i = s^E_{ij}T + d_{mi}E_m \quad (2)$$

where *m, k* = 1, 2, 3 (represents direction x, y, z); *i, j* = 1, 2, 3, …, 6 (4, 5, 6 represents the shear about the x, y, z axes); *S* = strain tensor; s^E = compliance tensor of piezo test at constant *E* condition; *T* = stress tensor; *d* = piezoelectric strain constant tensor; *E* = external electric field; *D* = charge displacement tensor; ε^T = permittivity/dielectric constant tensor measure at constant *T* condition.

The PEH can be designed in various modes which utilize the corresponding piezoelectric charge constant, d_{mi} where 'm' denotes the polarization direction of the piezoelectric layer, while 'i' denotes the direction of the stress or strain [15]. Hence, 31-mode PEH utilizes the d_{31} where the stress is perpendicular to its poling direction, while 15-mode piezoelectric utilizes the shear effect [16, 17]. Normally, $d_{15} > d_{33} > d_{31}$ [18].

1.2 Evaluation Factors

There are several ways to evaluate the performance of a piezoelectric transducer, such as direct measurement on the open-circuit voltage of a PEH. Some studies indicated using the measured power output across an optimum external load with impedance matching. To ensure a fair comparison, power density either per unit volume of piezo or per volume of device has been proposed. Besides, the electrical energy stored, U_E in a piezo can be calculated with the open circuit voltage and used as an evaluation factor [14].

The open circuit voltage in z-direction, V_3 is shown in Eq. (3). The details of formula can be found in [18].

$$V_3 = \int E_3 dt_p = \sum_{i=1}^{6} \int g_{3i} T_i dt_p \tag{3}$$

where g_{3i} = piezoelectric voltage constant; t_p = thickness of piezo.

The U_E and the total converted electric energy, U of the PEH can be calculated as shown in Eqs. (4) and (5).

$$U_E = \frac{1}{2} V^2 \frac{\varepsilon_{33}^T \varepsilon_0 A}{t_p} \tag{4}$$

$$U = \frac{1}{2}QV = \frac{1}{2}dg\sigma^2 At_p \tag{5}$$

where A = surface area of the piezo; Q = accumulated charge on the electrode; d = current constant; g = voltage constant; and σ = loaded stress [18].

It is noticed that the converted electric energy will increase with the product of ($d{\cdot}g$) from Eq. (5). Hence, another evaluation factor for PEH is the transduction rate of the piezo which is governed by the effective piezoelectric voltage and field constant, g^{eff} and d^{eff} [19].

Moreover, the efficiency of PEH can be evaluated by its ability to convert mechanical energy into electrical energy through the energy harvesting efficiency (or energy conversion efficiency), η, the electromechanical coupling factor, k and the energy transmission coefficient, λ_{max} as shown in Eqs. (6) - (10) [20-24].

$$\eta = \frac{E_{out,avg}}{E_{in,avg}} \times 100\% \tag{6}$$

$$E_{in,avg} = \frac{1}{T}\int_0^T Fd(t)dt \tag{7}$$

$$E_{out,avg} = \int_0^T P_{avg}dt = \int_0^T \frac{V_{rms}^2}{R}dt \tag{8}$$

$$k^2 = \frac{U_E}{W} \tag{9}$$

$$\lambda_{\max} = \frac{Q_s V_0}{4W} \tag{10}$$

where $E_{out,avg}$ = average output electrical energy, $E_{in,avg}$ = average input mechanical energy, F = applied force; d = displacement; T = period; P = output power; V_{rms} = root mean square of output voltage; R = external load resistance; W = work done by the external force in short circuit condition; Q_s = electric charge in short circuit condition; V_o = electric potential in open circuit condition.

Besides, by incorporating the structural design of MAS into the PEH, the piezo will experience more significant deformation due to the amplification effect under higher stress levels. Hence, computing the force or displacement amplification factor of the MAS based on the input and output ratio can be done as well for evaluating the energy harvesting performance of a PEH. It is suggested to use a constant evaluation factor while comparing the PEH or MAS under the same forcing environment.

1.3 Mechanical Amplifier Structure

Fig. 1 shows several MAS which can be generally classified into three main types, namely a cantilever type, a flexure type, and a combination multistage type.

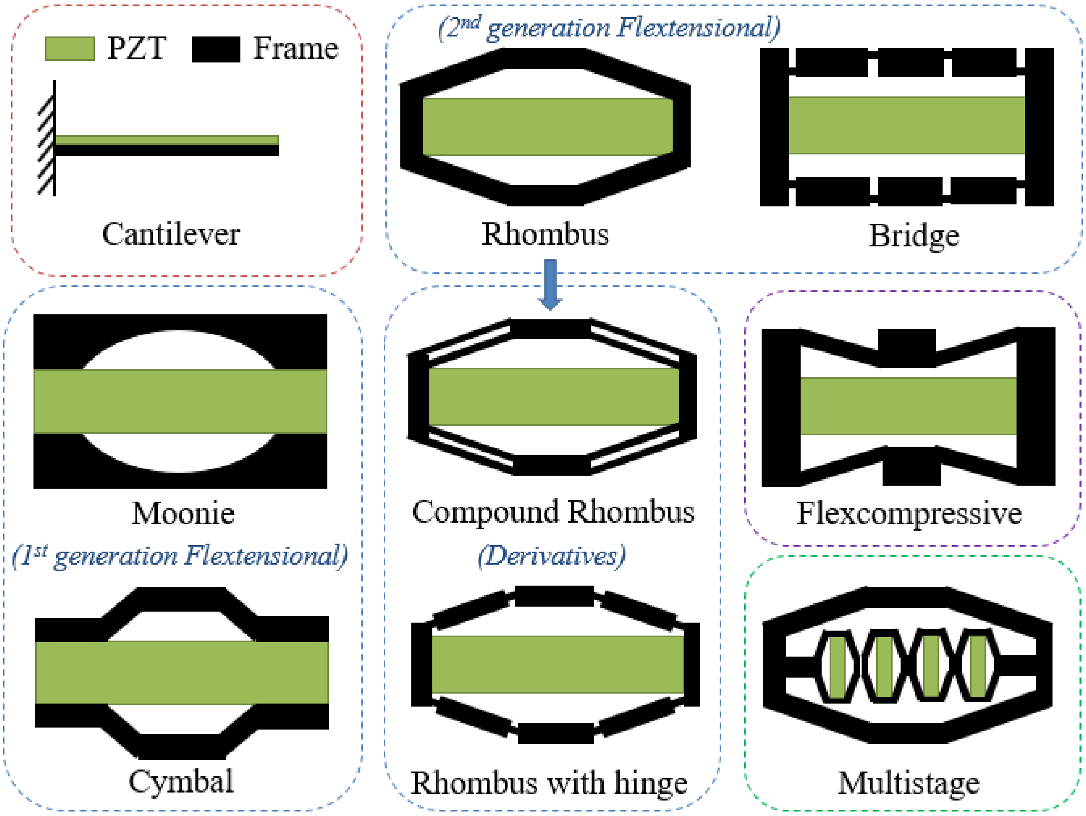

Fig. 1 Various types of MAS in the piezoelectric transducer

The objective of this article is to present a comprehensive review on the development of MAS of piezoelectric transducers starting from 2000 to date. The MAS is firstly classified by the deformation mechanisms, such as deflection (Cantilever), extension (Flextensional), compression (Flexcompressive), or combination (Multistage and combined structures), and then further divided into the derivative designs such as compound design and hinge design. Other manipulation factors that affect the power output of the PEH are discussed as well, such as the effect of proof mass, beam shape, piezo mode, magnetic field, etc. The characteristics and mechanisms of MAS have been presented in Sections 2 – 6, ranging from low force to high force environment. A summary of the harvesting performance and amplification factor has been illustrated in tabular form in the comparison section. The figures of merit have been plotted accordingly for various PEHs under a range of frequency and forcing amplitude with a proposed constant evaluation factor. This comprehensive comparison in terms of the energy harvesting performance, amplification effect, and also the pros and cons of the MAS, is aimed to provide guidance and ease the benchmarking process for future research.

2. Cantilever Structure

The cantilever beam is the most popular and basic structure in the piezoelectric transducer due to its simplicity and low cost. It consists of a thin layer of piezo, normally rectangular PZT, bonding with a substrate layer, such as a metal plate. One end of this structure is fixed while the other end is free for any forcing function, probably from the vibration source or the induced vibration due to the flow of wind to act on it [25, 26]. The cantilever structure has an advantage as its resonance frequency is much lower, thus a large mechanical strain can be formed when it is excited at its resonance frequency from a relatively small force [15].

2.1 Conventional Cantilever & Proof Mass

The cantilever structure is named according to the number of piezo layers. A rectangular cantilever with one 31-mode piezo layer is named 'Unimorph' as shown in Fig. 2 (a). 'Bimorph' structure is constructed with two piezo layers that sandwich the metal plate while the 'Multimorph' is constructed with more than two piezo layers. The power output of 'Bimorph' is doubled that of the 'Unimorph' without a significant change in the device volume [27]. The substrate layer in this cantilever structure is essential to move the neutral plane away from the middle of the piezo layer (preferably, outside the piezo layer) to minimize piezoelectric charge cancellation. No net charges can be generated if the strain neutral plane is in the middle of the piezo layer since the strain/stress is of opposite signs but the same magnitude above and below the neutral plane. The optimal positioning of the neutral plane increases with increasing thickness of substrate layer as the piezo layer is further away from the strain neutral axis and therefore increases the induced voltage [28, 29].

Conventionally, the cantilever structure has a narrow bandwidth where the beam oscillates in a smaller amplitude once the excitation frequency shifts away from the resonance frequency [30]. A proof mass is attached at the free end to tune the resonance frequency by changing its mass, size, and location [31]. The power output of a cantilever PEH is proportional to the attached proof mass as it increases the average strain energy [32]. Hence, the proof mass should be maximized within design constraints such as the size and beam strength. A torsional mode cantilever can be achieved by using a pair of asymmetry proof mass which is placed at different distances to the neutral axis [33] or using a rotator [34] as shown in Fig. 2 (b). It improved 30% of energy harvesting performance and had a wider bandwidth. An impact engaged 2 degree-of-freedom (DOF) harvester was proposed to enhance the dynamic motion of the cantilever during the in-phase mode where a larger impulse will be imparted on the tip mass as shown in Fig. 2 (c) [35].

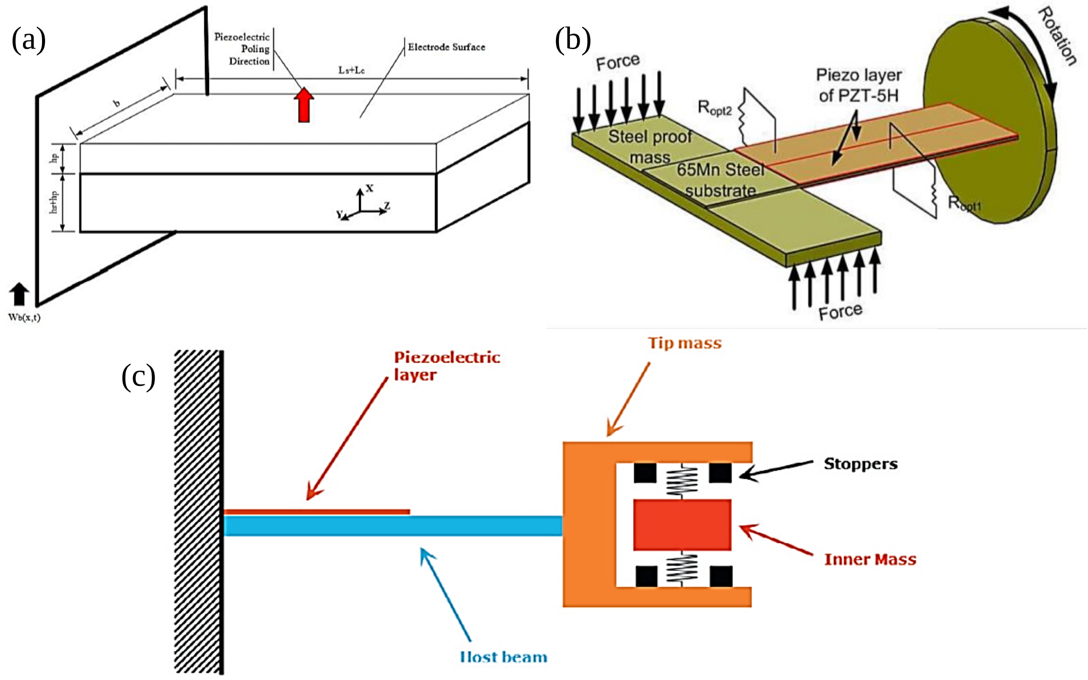

Fig. 2 (a) Conventional 31-mode Unimorph cantilever PEH (reprinted from [36], Copyright (2019), with permission from Elsevier); (b) Bimorph PEH in torsional mode (reproduced from [34]); (c) 2DOF harvester with stoppers (reprinted from [35], Copyright (2018), with permission from Elsevier)

2.2 Beam Shape

The power output of PEH is largely dependent on the volume of piezo subjected to mechanical stress. Generally, the stress is maximum at the fixed end and decreases while moving away from the clamp. Thus, the non-stressed part does not generate much power output [27] and can be removed as shown in Fig. 3.

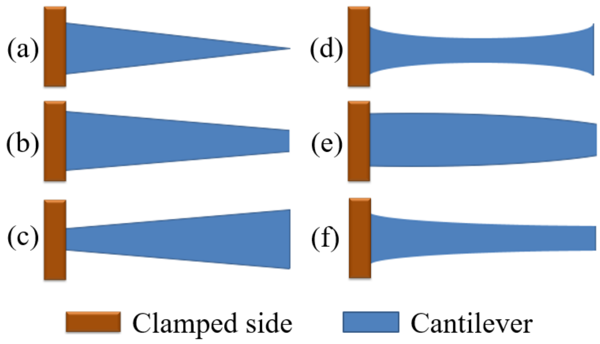

Fig. 3 Top view of the (a) triangular, (b) tapered, (c) reverse tapered, (d) quadratic, (e) trigonometrically tapered, and (f) exponentially tapered cantilever beam shape

A tapered or triangular shape transducer may achieve constant strain levels throughout the length of the piezo [37, 38]. A tapered cantilever PEH managed to harvest more than twice the energy than the rectangular cantilever due to the rise in bending energy [39, 40]. A triangular cantilever showed 25% higher strain and deflection than the rectangular beam with same base and length dimensions [41]. However, Dietl and Garcia [42] presented tapered and reverse tapered cantilever PEHs had slightly lower power output than the rectangular beam with the same beam length of 60 mm. Benasciutti, Moro [43] performed a fair comparison among the rectangular, tapered, and reverse tapered structures under two cases. Both tapered structures in case I (same resonance frequency and volumes) were having lower power density (-13.3% and -6.7%) than the rectangular cantilever; while structures in case II (same width of 14 mm) had improved the power output up to 24% and 113% respectively. The reversed tapered cantilever had greater power density than the tapered structure in both cases as the stress at the fixation had been significantly improved. The large area free end could be facilitated to locate the proof mass. Another cantilever structure that extended the rectangular shape with a reversed tapered shape at the free end, which named as ‘Trapezoid with Corners’ structure, had shown a higher strain and power output than the reversed tapered PEH [44]. A quadratic shape cantilever PEH was developed which scavenged two times energy than a rectangular cantilever [45]. Besides, a trigonometrically tapered or exponentially tapered cantilever had up to 45% greater buckling and flutter capacities than the rectangular beam [46]. A slope angle of 0.94° is tapered along the thickness of the beam which has more evenly strain distribution and power amplification factor of 3.6, but it will have manufacturing difficulty [18].

Fig. 4 (a) - (c) shows three beam shapes, namely, T, Pi, E-shaped which are compared with a rectangular cantilever. Although the rectangular cantilever had the highest power output of 87 μW, the E-shaped cantilever showed the best performance with the highest displacement of 0.61 μm and a power output of 49 μW [47]. A 7-layers Zigzag beam PEH with an inclined angle of 12° was proposed which can be excited from 3 axes as shown in Fig. 4 (d). Maximum powers of 180 μW, 88 μW, and 56 μW were generated when exciting in vertical, horizontal, and longitudinal directions. The 3-dimensional PEH can realize a wide bandwidth, high acquisition efficiency (multi-directional harvesting function), and high fatigue life [48]. Another spiral structure PEH was proposed to achieve 3-dimensional energy harvesting with an arc-shaped PZT (around 30 × 6 mm^2) placed near to the free end. As the radian of spiral (number of rotations) increases, the resonance frequency becomes smaller. An output power of 75 μW is produced with a 4π radian spiral cantilever PEH at its resonant frequency of 52 Hz [49]. A 2-directional flexible longitudinal Zigzag structure [50] and the multi-branch structure [51], had been proposed for the low-frequency vibration source. Fig. 4 (e) shows a 31-mode arc-curved PZT was merged on the cantilever PEH with higher and more uniform distributed stress. It showed 2.55 times and 4.25 times higher power than the plain cantilever PEH for the one half-tube and two half-tubes PEH [52]. Another research found that adding an intermediate auxetic booster between the PZT and the cantilever beam can induce extra stretching strain on the PZT in two perpendicular directions of the same surface, which utilizes the d31 constant better. The two auxetic structures, AS-I and AS-II, can increase the power output by factors of 3.9 and 7.0 respectively as shown in Fig. 4 (f) [53].

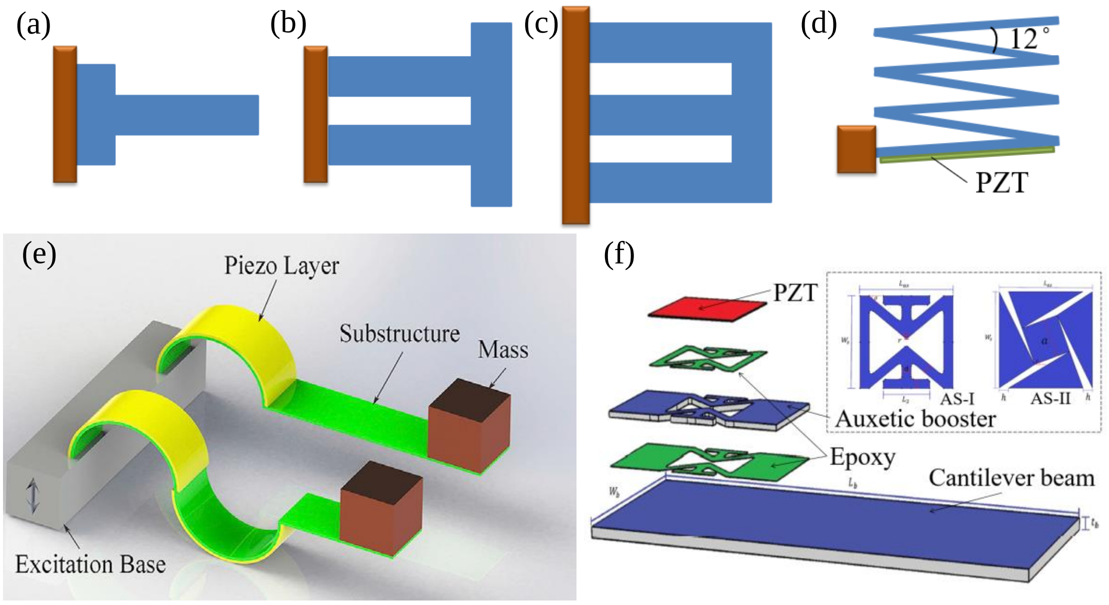

Fig. 4 Top view of (a) T-shaped, (b) Pi-shaped, and (c) E-shaped cantilever; (d) Side view of Zigzag cantilever; (e) Cantilever with curved PZT (reprinted from [52], Copyright 2017, with permission from Elsevier); (f) Cantilever with intermediate auxetic boosters, AS-I and AS-II (reprinted from [53], with permission from Wiley)

2.3 33- & 15-mode Cantilever

Since $d_{33} > d_{31}$, an interdigitated surface electrode design is introduced to achieve 33-mode piezo, but the poling treatment is complicated [27]. Another way is changing the orientation of the piezo by aligning the poling axis parallel with the stressing axis. Due to the limit of poling length in a piezo plate, a few segments of the piezo are combined and formed a piezoelectric multilayer stack (piezo stack). The d_{eff} of the piezo stack is the multiplication of d_{33} with the number of piezo layers and an efficiency constant [54]. For example, the d_{eff} of the PZT stack is 1.39×10^6 pC/N at resonance, which is larger than a single PZT layer ($<1 \times 10^4$ pC/N) with the assumption of 80% power transition efficiency for the PZT stack (0.8 of efficiency constant due to the electrode pattern, the protective layer of the stack and the clamp effect from the metal electrodes between the layers). The power density is significantly higher than a similar size cantilever type PEH and increases with the number of PZT layers [55]. Generally, the piezo stack is suitable for large force environment due to its high mechanical stiffness.

A 33-mode PZT stack is embedded with the cantilever structure to examine the effect of different length, thickness and number of PZT layer. The PZT layers were assembled in series but connected electrically in parallel to offer a larger electrode area, higher electric current, and lower impedance as shown in Fig. 5 (a). The stack design managed to decrease the natural frequency of the harvester. Meanwhile, increasing the length of PZT will lead to higher charge and voltage outputs [36]. Fig. 5 (b) shows a barbell-shaped PEH with a 33-mode ring-type piezo stack can overcome the failure of the epoxy bonding layer and sustain larger impacts [56]. Zhao, Zheng [57] proposed a cantilever harvester with two 15-mode piezo layers ($13.0 \times 2.5 \times 1.0$ mm^3) which were series-connected to utilize the shear effect. It had a greater power output than that with only one 15-mode piezo layer even in a larger size ($13.0 \times 6 \times 1.0$ mm^3). However, due to manufacturing difficulty in the polarization process which requires extremely high voltage, d_{15} is less utilized.

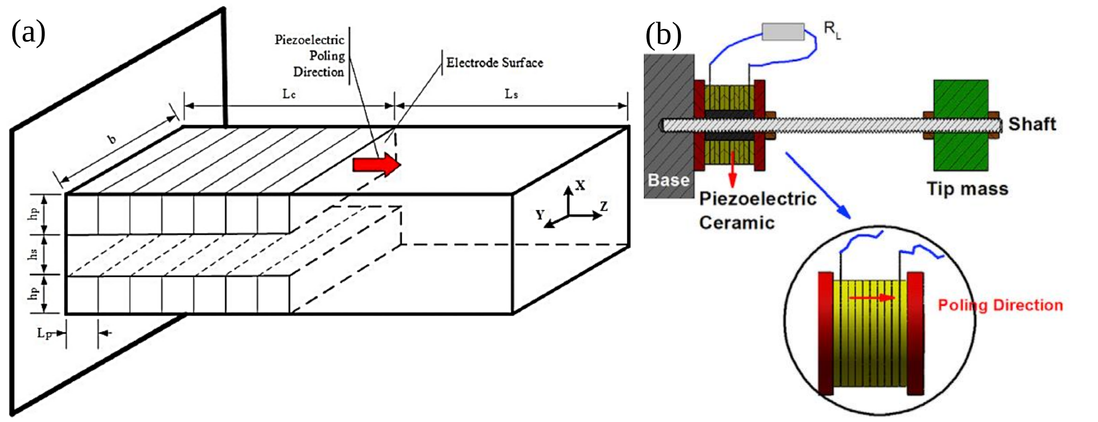

Fig. 5 (a) 33-mode PZT stack cantilever harvester (reprinted from [36], Copyright 2019, with permission from Elsevier); (b) Barbell-shaped cantilever harvester (reprinted from [56], with the permission of AIP Publishing)

2.4 Magnetic Tunable Cantilever

Challa, Prasad [58] proposed a magnetic field tunable cantilever PEH to alter the stiffness and tune the resonance frequency from 26 Hz to a wider working frequency bandwidth (22 - 32 Hz) with a power output of 240 - 280 µW. The nonlinearity of PEH induced by magnetic forces is usually classified into three main categories, namely, monostable, bistable, and tristable [59]. Harne and Wang [60] then presented the difference between magnetic attraction and repulsion bistable harvester (2 stable and 1 unstable equilibrium positions). Fig. 6 (a) shows a magnetic attraction PEH which can be multi-stable based on the angular orientation of the external magnets [61]. An asymmetric U-shaped cantilever was adopted to exhibit a magnetic nonlinearity with multimodality as shown in Fig. 6 (b). It yielded a closer two resonance frequencies bandgap compared to the linear one without the two permanent magnets. Hence, this design shows higher energy output, lower and closer resonance peak [62].

To broaden the bandwidth and increase the power output, several methods had been proposed to introduce nonlinearities onto the PEH such as applying parametric excitation, using multi-degree-of-freedom approaches (with more than one cantilever beam with magnetic tips), utilizing movable magnet, using axial static preload to optimize the stiffness of the structure, and using stoppers to realize a spring hardening effect [63]. For example, two stoppers are added to an inverted cantilever to confine the beam's deflection range so that the elastic force dominates the magnetically attractive coupling employed in the PEH, making the device monostable as shown in Fig. 6 (c) [64]. By altering the spacing between the tip mass and the external magnets, the operating frequency can be tuned [65]. Zhou, Cao [66] used rotatable magnets to obtain a broad low-frequency range of 4 - 22 Hz within a compact design by altering the inclination angle of the magnet. Compared to linear PEHs that have poor performance away from their natural frequency, nonlinear PEHs perform better because they capture vibration energy over a broader spectrum, which is in a wider frequency band [63]. The nonlinear PEH is less sensitive to the change of excitation frequency than the linear PEH, making it more suitable for harvesting energy from ambient vibration in practical applications [67].

A non-contact magnetic plucking is induced to achieve frequency up-conversion in a knee-joint PEH as shown in Fig. 6 (d). The knee-joint motion will excite the 8 Bimorphs PEHs through the repulsive force between the primary magnets (PM) and the secondary magnets (SM). The repelling configuration produced 3.6 times higher energy output than the attracting configuration. An average power output of 5.8 mW was generated under a knee-joint motion at 0.9 Hz [68]. A tapered cantilever was then integrated with the non-contact magnetic plucking mechanism and formed a rotational PEH. It was applied in the wind energy harvesting field, where the magnets were fixed at the tips of the fan blades while the tapered cantilever with a tip magnet was placed at the fan frame. Experimental results show that it could generate a power output of 0.64 mW/cm^2 at rotational speed of 400 r/min, which is 1.6 times larger than that of a rectangular cantilever. This structure can also avoid damage of the piezo elements caused by direct impacts due to the non-contact mechanism [69]. In short, the frequency up-converting mechanism that utilized techniques, such as freely moving mass, plucking mechanism and mechanical impact, or focused on the structure characteristics, such as gear transmission and direct load structure, could improve the harvesting efficiency for low-frequency vibration, effectively expanding working bandwidth, and reducing volume of harvester with increasing energy density [70].

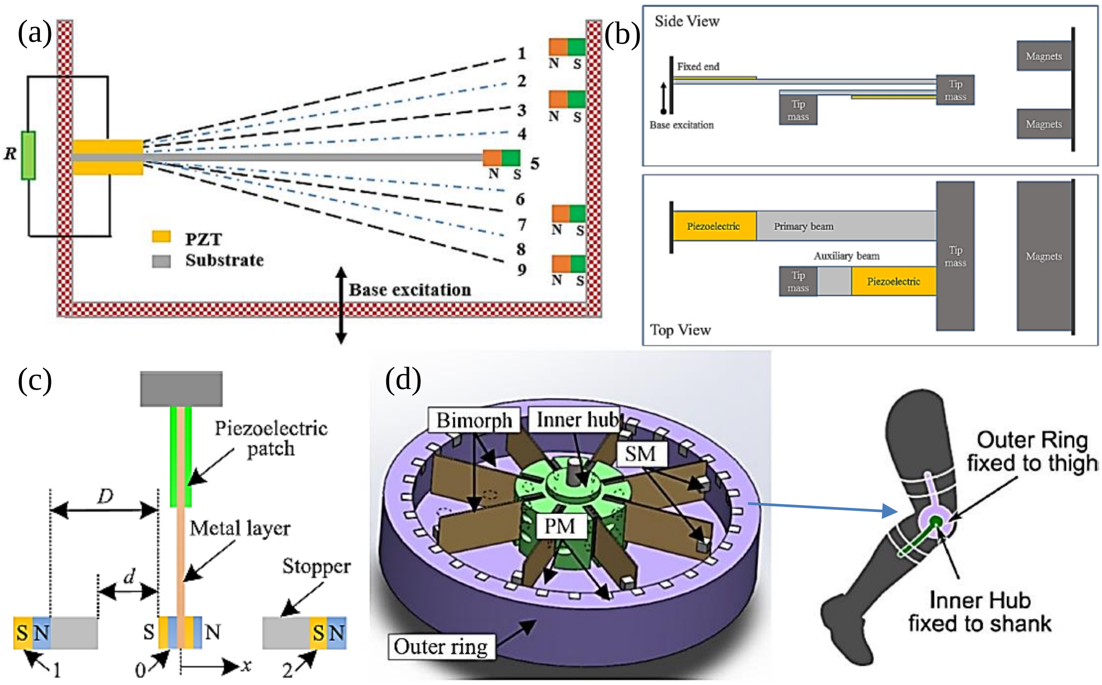

Fig. 6 (a) Structural schematic of a magnetic attraction multi-stable PEH (reprinted from [61], Copyright 2018, with permission from Elsevier); (b) Asymmetric U-shaped magnetic repulsion PEH (reprinted from [62], Copyright 2018, with permission from Elsevier); (c) Vertical Bimorph cantilever PEH in a magnetic field with two additional stoppers (reprinted from [65], Copyright 2018, with permission from Elsevier); (d) Schematic diagram of knee-joint PEH with frequency up-conversion induced by magnetic plucking (reproduced from [68])

2.5 Pre-stressed & Edge-clamped

Reduced and Internally Biased Oxide Wafer (RAINBOW) and Thin Layer Unimorph Driver (THUNDER) are two pre-stressed transducers. RAINBOW consists of a piezo layer and an oxygen reduce layer [71]. However, it is more brittle and not suitable for high force roadway environments [20]. THUNDER is constructed by sandwiching the piezo layer with aluminium and stainless steel layers which are heated and cooled rapidly. The difference in thermal expansion coefficients introduces the pre-stress in the piezo layer [72]. THUNDER structure has higher block force, displacement, and fatigue life, which can withstand higher force up to 0.5 MPa [20]. It has been used in actuator mode to control the curvature and hence the tuned frequency. In 2022, an analytical model of the THUNDER PEH had been developed based on the dynamic stiffness method to predict its measured output, such as magnitude, phase, Nyquist plots, and resonance frequency shift with high accuracy [73].

Other than the deflection of cantilever caused by the vibration source, bending mode Bimorph had been introduced to scavenge energy from human knee motion through a slider-crank mechanism, where one end was fixed at the upper leg whereas another end was at the lower leg. The two layers of flexible MFC could generate a maximum average power of 13.2 mW at normal walking speed of 4 km/h as the bending Bimorph was compressed and released periodically [74]. Umeda, Nakamura [75] developed a pressure mode all edge clamped circular PEH with a piezo disc bonded to a bronze disc with high stiffness. The two sides of the diaphragm must be isolated to create stress in response to a pressure change in the surrounding medium [76]. The power output is 1 - 20 mW, which is higher than a cantilever but lower than a flextensional PEH [15].

3. First Generation Flextensional Structure

Cantilever typed harvester may achieve high power output under its resonance mode. However, long term excitation at its natural frequency may lead to a shorter lifetime as fatigue may occur due to its weak mechanical strength [19]. The flexure structure with higher robustness and magnification function converts the transverse input force into larger lateral tension or compression output force acting on the piezo which improves the power output from μW/device up to tens of mW/device [15]. It can be divided into flextensional and flexcompressive structure based on the direction of the deformation either away or towards the middle node under the commonly used compressing downwards force.

3.1 Moonie, Cymbal & Rectangular Cymbal

Moonie structure is constructed with two half-moon shaped metal end-caps to protect the PZT under high stress level as shown in Fig. 7 (a) [77, 78]. Fig. 7 (b) shows a Cymbal structure is designed to reduce the stiffness of the Moonie frame and stress concentration in the PZT. Thus, the allowable applied stress and the displacement can be increased [20]. The Cymbal structure comes in circular and rectangular shapes as shown in Fig. 7 (c) and (d), where the rectangular-shaped Cymbal is named as 'Rectangular Cymbal' (to differentiate with the general circular 'Cymbal') in this paper and 'Bridge' in some papers. Fig. 7 (e) and (f) show a metal ring and threaded bolts are used to avoid the asymmetries configuration and improve the mechanical coupling effect instead of using epoxy adhesive only [79].

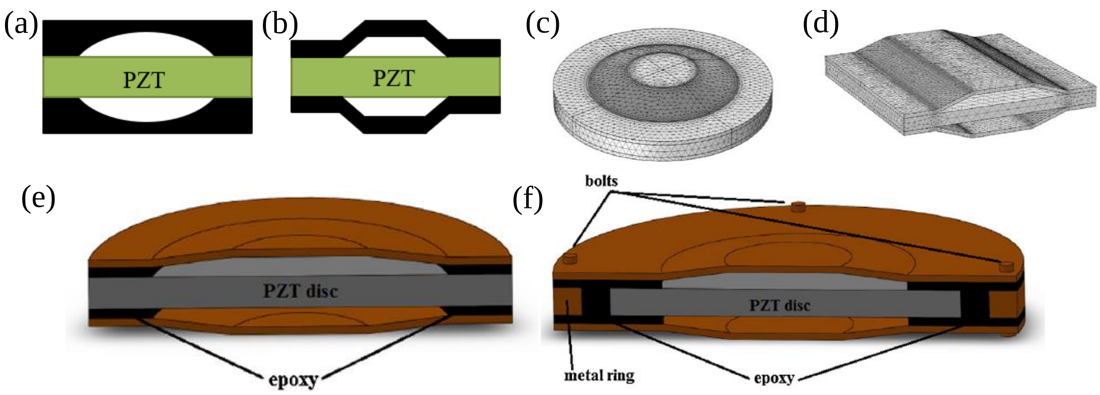

Fig. 7 (a) Side view of Moonie and (b) Cymbal; (c) The structures of conventional circular Cymbal and (d) Rectangular Cymbal (reprinted from [80], Copyright 2017,

with permission from Elsevier); (e) Conventional epoxy bonding in Cymbal structure; (f) Reinforced bonding with retarded metal ring and bolts design (reprinted from [79])

A strain amplification factor ($\approx Ø_c/2h$) of 8.5 was calculated for the Cymbal structure based on the cavity height, h and cavity diameter, $Ø_c$ [19]. The authors also tested several types of PZT material. The D210 PZT shows the highest voltage output due to its higher g than the soft APC-850 PZT and hard APC-841 PZT. In another study, PZT-5H shows the highest ($d \cdot g$) values in both 31 and 33-mode while PZT-5A has the highest ($d \cdot g$) value in 15-mode as compared with PZT-2, PZT-4, and PZT-8 [20]. A Cymbal structure shows an amplification factor of 16 - 22 based on the voltage output of a standalone PZT layer under an impact force [81]. Liu and Wang [82] adopted the PZT stack design by having two PZT rings and three metal rings alternatively in the Cymbal structure to improve the power output in high force roadway environment as shown in Fig. 8 (a).

Zhao, Yu [14] selected the ordinary Cymbal PEH to harvest energy from asphalt pavement due to its low cost, high reliability, and reasonable efficiency. A bury depth of 40 mm and contact stress of 0.7 MPa (25 kN/tire) were set in the FEA. Increasing the diameter of Cymbal will enhance the voltage but decrease efficiency. The maximum output power was 1.2 mW with the assumption of 20 Hz vehicular frequency. 200 kW of harvested electricity had been reported from one lane-mile of highway in Israel and China which exhibited the possibility of roadway PEH application [83]. Another study shows that one Cymbal PEH can generate 16 µW for the pass of one heavy vehicle wheel as shown in Fig. 8 (b). 40 - 50 MWh/m^2 energy density can be obtained from 100 m road with the use of 30 thousand cymbals, which can account for >65 MWh annually [84].

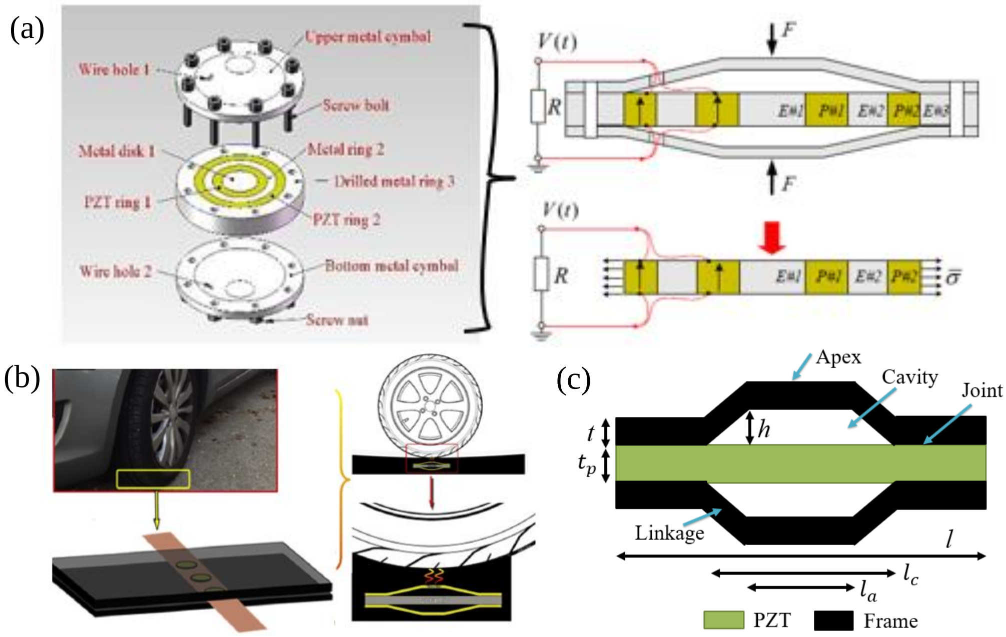

Fig. 8 (a) Radially layered 31-mode Cymbal PEH (reproduced from [82]); (b) Vehicular loading of the wheels deform the asphalt and excite the Cymbal PEHs which are embedded in the pavement (reprinted from [84], Copyright 2016, with permission from Elsevier); (c) Schematic of a Rectangular Cymbal PEH

Rectangular Cymbal has the highest values of V, W_l, U_E, k, and λ_{max}, followed by the Cymbal and lastly the Moonie under the roadway condition [20]. Kim, Batra [19] agreed that the Cymbal structure was preferred over the Moonie in terms of low fabrication cost, high stability under high loading force, and large displacement. The Cymbal structure with higher $d^{eff} \cdot g^{eff}$ was more efficient than the cantilever PEH. The flextensional structures are recommended for roadway application because of their reasonable efficiency and stiffness compared to the THUNDER and a standalone PZT stack even they have higher k and λ_{max} values. The PEH should have the same stiffness as the pavement to reduce its influence on the pavement. Moonie has a lower efficiency [20] and thus Cymbal and Rectangular Cymbal structures are recommended for energy harvesting in high force environment, such as under floor tiles, shoes, roadway pavement, or machine suspensions, due to its inherent structure.

3.2 Slotted Cymbal

A slotted Cymbal is developed to release high circumferential stress and minimize the loss of input energy. More radial slots up till the slanted part of the Cymbal had been designed, which is named as cone radial slot. The power output was 0.6 times higher than the ordinary Cymbal. The output voltage and power increased with the number and length of radial slots [85]. A circumferential slot had been tested with various depths which produced 0.8 times higher power than the ordinary Cymbal. However, the slotted design will reduce the rigidity of Cymbal and difficulty may arise during the fabrication process [86].

3.3 Addition of Substrate

Fig. 9 (a) shows the PZT cracks at the contact area with the Rectangular Cymbal under 0.8 MPa [20] as the stress concentrations exceed the yield strength of PZT, which is 35 MPa [87]. An additional steel substrate which is 8.38 times thicker than the PZT, is introduced to reinforce the PEH and work safely under 1940 N. However, most of the input energy has absorbed by the substrate, causing a low power output of 121.2 μW [88, 89]. Daniels, Zhu [90] then proposed dual-layer substrates with a lower thickness that sandwiched a 31-mode PZT to achieve the shielding effect from both sides and increase the load capacity as shown in Fig. 9 (b) and (c). Fig. 9 (d) and (e) show the overall stress has been reduced with the addition of dual-layer substrates [9, 87].

Luo, Liu [91] then used sequential quadratic programming to optimize the parameters of the PEH. Rectangular Cymbal structure was used to fully utilize the best orientation of piezo materials. It is then applied as a footwear PEH as shown in Fig. 9 (f). The ideal force amplification ratio of the Rectangular Cymbal is calculated based on the kinematic mechanism. It is equal to cot θ where θ is the end-cap internal angle, which is agreed by Li, Guo [92]. The end-caps will amplify the incident force when θ <45°. However, there is an optimum angle which is 15° in this design as the amplification factor will reduce when the inclined linkages are shortened by the large forces at an extremely small angle. The optimum configuration should be evaluated by considering the balance between energy harvesting performance and mechanical failure potential due to stress concentrations. For example, minimizing the end-cap thickness can maximize the power output, but a thicker end-cap can withstand a higher loading force [9].

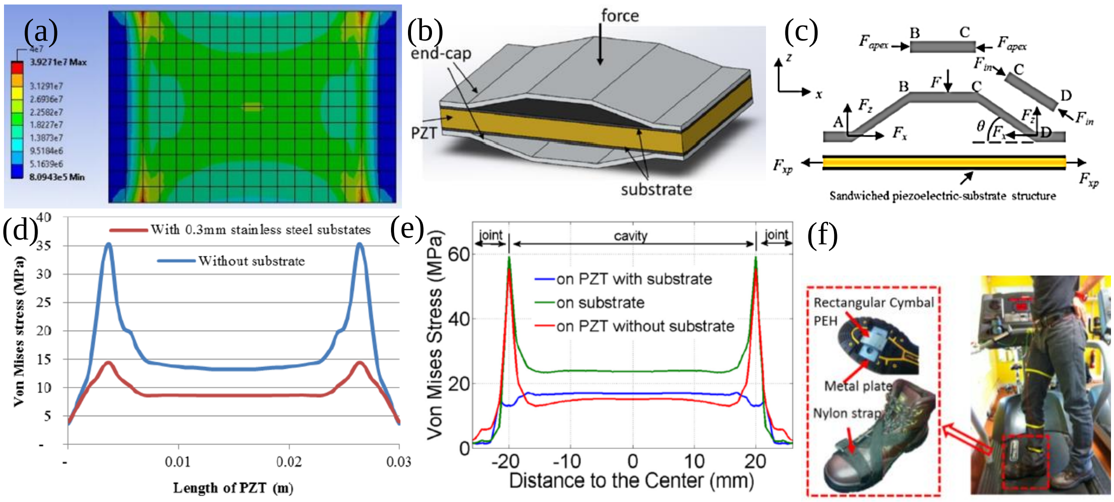

Fig. 9 (a) Stress distribution of the PZT plate under high loading force (© 2019 IEEE. Reprinted, with permission, from [87]); (b) & (c) Rectangular Cymbal PEH with dual layer of substrates and its force amplification mechanism (reproduced from [9]); (d) & (e) Stress distribution of the PZT plate along the length of PZT with and without substrates [9, 87]; (f) Experimental setup for testing the Rectangular Cymbal PEH as a footwear energy harvester [9]

3.4 33-mode Rectangular Cymbal

Fig. 10 (b) shows a Rectangular Cymbal structure with a seven-layer parallelly connected 33-mode PZT-5X stack, which has a higher ($d \cdot g$) value than PZT-5H. It produces four times energy than the traditional 31-mode Rectangular Cymbal PEH. The thickness of the end-cap and PZT, as well as the cavity height, are the key factors in optimizing the performance of PEH. It is demonstrated as a roadway PEH by having 64 parallel-connected Cymbal PEHs assembled in a 177.8 × 177.8 × 76.5 mm^3 Aluminium casing as shown in Fig. 10 (c) [80].

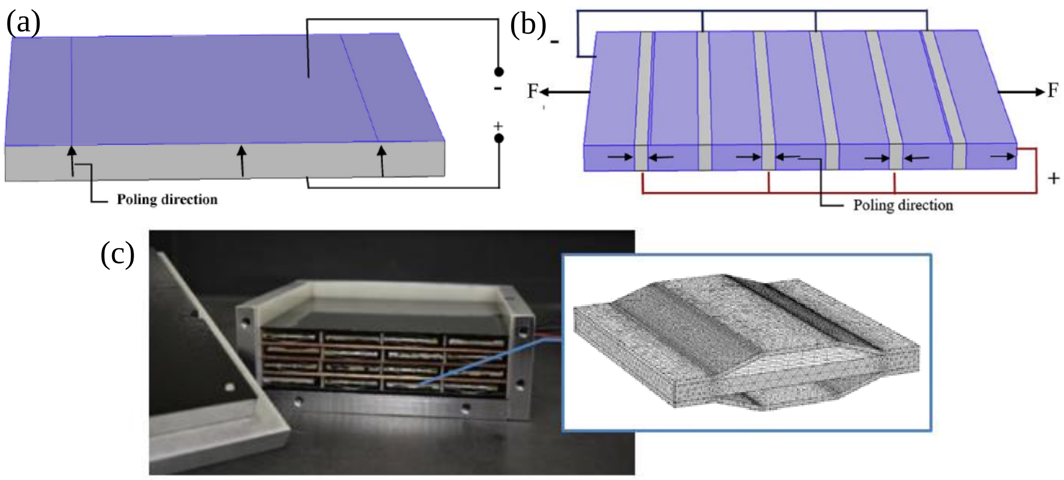

Fig. 10 (a) 31-mode conventional PZT; (b) 33-mode parallelly connected PZT stack; (c) Prototype of a roadway PEH with 64 33-mode Rectangular Cymbal transducers (reprinted from [80], Copyright 2016, with permission from Elsevier)

3.5 Arc & Arch Cymbal

Two arc shape rectangular Cymbal structures are designed to mitigate the effect of stress concentration as shown in Fig. 11. The maximum electric potential of the Arch is higher than the Arc, followed by the Rectangular Cymbal. The voltage drops with higher modulus and thicker end-cap. In terms of load capacity, the Rectangular Cymbal has a maximum load at 1 MPa, followed by the Arch of 0.8 MPa and Arc of 0.7 MPa. The Arc is fragile due to its large maximum tensile stress and shear stress, whereas the Arch has high durability, strong capability to resist pressure, and high energy conversion efficiency to work as a pavement PEH [93]. However, the bonding strength and technique should be improved to cope with the shear stress [94]. A circular Arch end-caps are bonded to the Brass rings, then to the PZT disc and demonstrated as a shoes PEH. However, the Brass rings will reduce the transmission of energy to the PZT disc. The capacitance of the component will increase with a larger area of PZT but a smaller thickness of PZT. Hence, the matching impedance will reduce, result in higher power output and a lower force demand [95, 96].

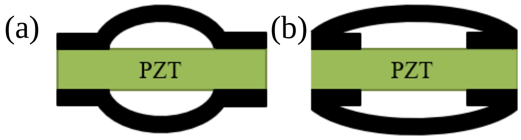

Fig. 11 Side view of the (a) Arc and (b) Arch Rectangular Cymbal structure PEHs

3.6 Combined Structure

It is difficult to excite the high-stiffness Cymbal PEH at its high resonance frequency as the ambient vibration sources normally are below 300 Hz [97]. Xu, Ren [98] combined a high flexibility Cantilever beam with two Rectangular Cymbal structures, which named as CANtilever Driving Low frequency Energy harvester (CANDLE) as shown in Fig. 12 (a). It produced high power output at a low frequency, which is 4.9 times higher than the Cymbal PEH. The proof mass can convert more electrical energy from vibration sources and lower the natural frequency [99]. Tufekcioglu and Dogan [100] applied the CANDLE concept with two circular Cymbal PEHs which consisted of a 31-mode two-layer-stacked PZT-5H disc each as shown in Fig. 12 (b) and (c). But the harvesting performance is lower than the rectangular CANDLE.

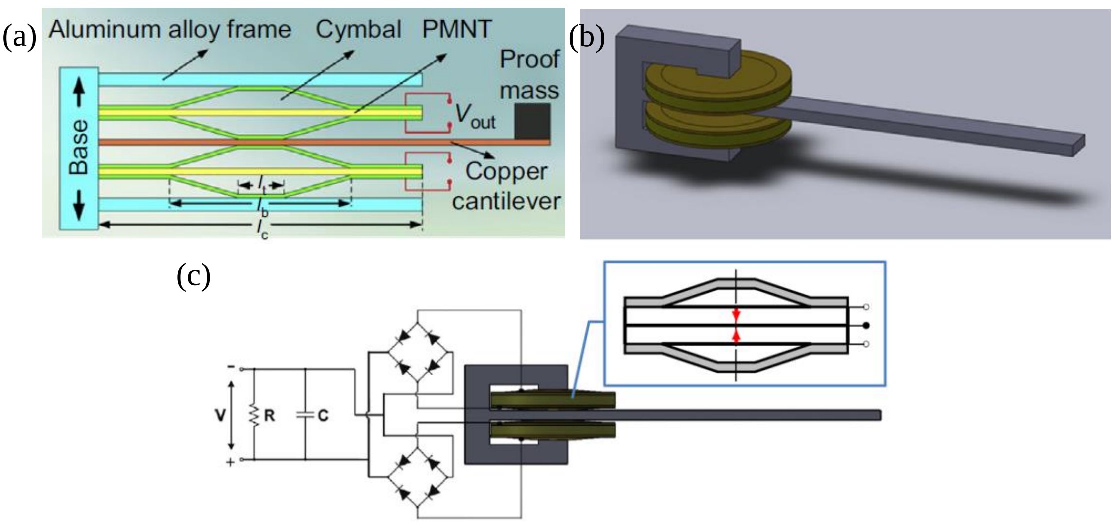

Fig. 12 CANDLE based on a pair of (a) rectangular Cymbals (reprinted from [98], with the permission of AIP Publishing) and (b) a pair of circular Cymbals with (c) 31-

mode two-layer-stacked PZT-5H disc (reprinted from [100], Copyright 2014, with permission from Elsevier)

Zou, Zhang [101] introduced a nonlinear magnetic repulsive force by placing a Rectangular Cymbal PEH with magnet opposite to the free end of the Cantilever to increase the bandwidth and power density. With the magnetic pressure exerted on PEH as the beam oscillated, the PZT was subjected to a tensile force. Zou, Zhang [102] used another two PEHs as stoppers which can limit an unwanted large displacement of the tip magnet as shown in Fig. 13. The energy loss caused by the magnetic stoppers was smaller than the collision stoppers. This design improves the harvesting performance from low-frequency weak vibrations source.

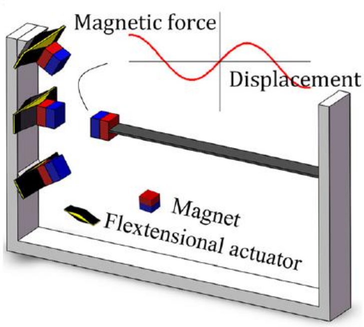

Fig. 13 Combined structure of cantilever and flextensional transducers with nonlinear magnetic repulsive force (reprinted from [102], with the permission of AIP Publishing)

3.7 Compressive Mode Cymbal

Since the compressive yield strength of piezo is 10 times higher than its tensile yield strength which can be up to 600 MPa (270 MPa vs 35 MPa, estimated by STEINER & MARTINS, Inc), the compressive mode PEH is designed to withstand higher force [103, 104]. A 31-mode PZT ring is compressed through an inner flextensional Cymbal structure to increase the power output and eliminate the bonding failure issue with an outermost retaining ring. The PZT ring is replaced by four 33-mode PZT stacks to further increase the power output [105]. Two coil-type 33-mode PZT stacks are twined at the two ends of the Rectangular Cymbal with an outermost shaft that pre-compressed them. Larger electric voltage and power output are produced if compared with Bimorph or tensional Cymbal PEHs [92].

Another compressive mode Rectangular Cymbal PEH with two 33-mode PZT stacks was designed to sustain under heavy loads [106]. Two compressive mode PEHs were combined and connected by a supported beam, which acted as a shared loading platform. It showed over 400% harvested energy if compared with two independent compressive mode PEHs [107]. In short, compressive mode PEH has higher load capacity, lower resonance frequency, and higher power density than the conventional PEH included the standalone PZT stack. However, this design required the PZT to be placed outside of the end-caps, resulting in a bulky design.

3.8 Compressive Mode Combined Structure

Yang and Zu [10] developed a compressive mode Rectangular Cymbal PEH using the cantilever beams and proof mass to increase the power output and wider the bandwidth as shown in Fig. 14. When the PEH is excited under a base vibration, the mechanical energy is absorbed by the elastic beams and mass blocks. A pulling force is then induced on the end-caps as the cantilever oscillates, resulting in compressive stress in the PZT. The Rectangular Cymbal can generate 100% higher voltage than a circular Cymbal as higher effective stress is found in the rectangular PZT [104]. A force amplification ratio of 6.3 is reported for the Rectangular Cymbal structure at 6.34° [103]. The hinge design at the clamped connection between the cantilever ends and the base as well as the proof mass can reduce the stiffness and enlarge the deflection. The fully hinged PEH had 3 times higher voltage output, 15% lower natural frequency, and 37% broader frequency bandwidth, compared to the clamped design [108]. Wang, Yang [109] then integrated this combined structure with a rotary magnetic plucking mechanism, which increased the voltage output by around 250% and could be applied in automobile tires, jet engines, and wind turbines in the future.

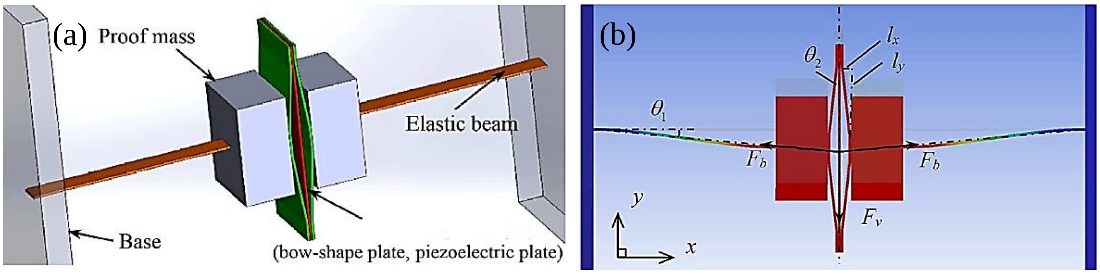

Fig. 14 (a) Isometric view and (b) front view of a compressive mode combined structure of Rectangular Cymbal and elastic beam with mass blocks PEH (reprinted from [10], Copyright 2014, with permission from Elsevier)

4. Second Generation Flextensional Structure

4.1 Rhombus

The second generation flextensional structure is designed to overcome the destructiveness of the first generation flextensional structure such as the bonding failure issue. Rhombus structure can achieve this by clamping the PZT plate from the vertical sides as shown in Fig. 15 (a). The ideal displacement amplification ratio, G_{ideal} of the Rhombus is equal to cot α, which is similar to the Cymbal structure as they share the same quarter model shown in Fig. 15 (b) [110]. In fact, the flexure linkage possesses both bending and longitudinal stiffness which causes elastic energy stored in the mechanism. The actual displacement amplification ratio, G_{actual} can be derived as shown in Eq. (11). A maximum amplification ratio of 9.47 is proven when the angle, α equals 3.04° [111].

$$G_{actual} = \frac{\Delta y}{\Delta x} = \frac{l_a \cos\alpha}{\dfrac{t^2\cos^2\alpha}{1.5 l_a \sin\alpha} + l_a \sin\alpha} \tag{11}$$

Ling, Cao [112] included the input stiffnesses (K_{in}, K_v, and K_{PZT}) of the compliant mechanism in the calculation, rather than the bending stiffness (K_θ) and translational stiffness (K_l) only. This is because the output displacement of a PZT stack will be reduced due to the preload if compared with the free-operating Rhombus structure. The calculated displacement amplification ratio, R_{amp} is 13.05, using Eq. (12), which is <10% deviated from the experiment.

$$R_{amp} = \frac{K_{PZT} K_v}{K_{PZT} + K_{in}} \times \frac{K_l L^2 \sin\theta \cos\theta}{12 K_\theta \cos^2\theta + K_L L^2 \sin^2\theta} \tag{12}$$

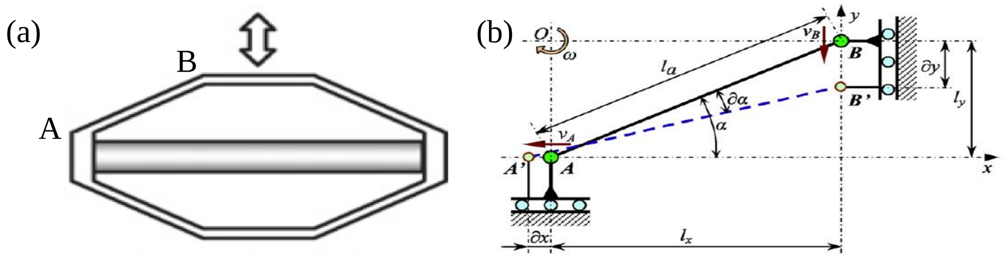

Fig. 15 (a) Rhombus structure PEH and (b) its quarter amplification mechanism kinematic model where α is the inclined angle (reprinted from [110], Copyright 2006, with permission from Elsevier)

4.2 Rhombus with Hinges

Zhou and Henson [113] proposed a Rhombus structure with additional hinges design at the four linkage arms. The hinges have lower thickness and less stiffness than the arms which ease the deformation of the frame. Fillet is designed to reduce stress concentration at the corner [114]. However, it has a lower load capacity and safety factor since the bending area is concentrated at the hinges [115]. Hence, the hinge design is suitable when large deformation and amplification ratios are desired under low excitation force. Feenstra, Granstrom [116] applied this structure in developing a compressive mode PEH which utilized the differential forces exerted in the straps of a backpack due to walking, as shown in Fig. 16. A tensional outward pulling force was applied to the Rhombus structure through the backpack strap and the piezo was being compressed by the extended part from the sides. This lightweight transducer backpack design only leads to minimal parasitic effects, making it a feasible method of gathering energy from human motion.

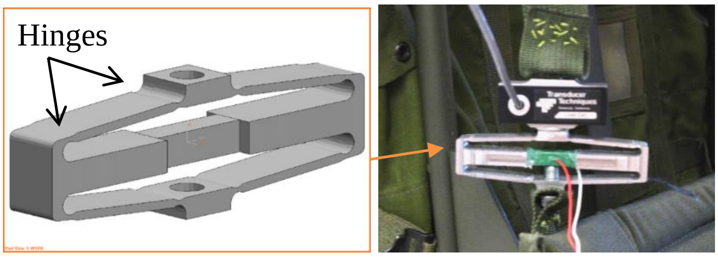

Fig. 16 Rhombus structure PEH and its backpack application (reprinted from [116], Copyright 2016, with permission from Elsevier)

4.3 33-mode Rhombus

A 33-mode Rhombus PEH with piezo stack which named as APA 400M is reported with lightweight (19 g) and compact size (48.4 × 11.5 × 13.0 mm^3) as shown in Fig. 17 (a) [117]. The poling directions are indicated as shown in Fig. 17 (b) [118]. It has three main advantages over the standalone PZT. Firstly, 48.6 times more mechanical energy is transmitted into the PZT through the Rhombus frame. Secondly, the energy conversion efficiency is about three to fivefold by utilizing a 33-mode PZT. Lastly, 26.5 times more electrical charge is generated through the parallel-connected PZT stack. By adding a 500 g proof mass on top of the structure, 328.34 mW can be generated at its natural frequency of 138.1 Hz. It is 164 times higher than a non-proof mass structure with natural frequency of 936 Hz [55].

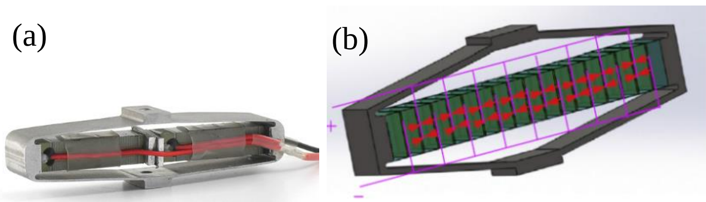

Fig. 17 (a) Cedrat, APA 400M (reprinted from [119]); (b) Parallel-connected PZT stack in Rhombus PEH (reprinted from [15], Copyright 2016, with permission from Elsevier**)**

4.4 Compound Rhombus

Compound Rhombus was designed to strengthen the PEH with higher stiffness and load capacity by increasing the beam number for the four arms. The distance between two adjacent beams was set at 1.5 mm to avoid manufacturing difficulty. The FEA force amplification factor was computed based on an input force of 400 N and the corresponding output force acted at the piezo, which equaled 4.33 for single beam design with a safety factor of 1.5. The four-beam compound structure had a lower amplification factor of 3.88 but a higher safety factor of 3.03. The maximum stress had been reduced and the safety factor had been enhanced with the increasing number of beams. However, the force amplification ratio was decreased, and the overall frame size was increased. Eventually, the two-beam compound Rhombus was adopted with an amplification ratio of 4.17 and a safety factor of 2.42 [115].

4.5 Combined Rhombus Structure

Two Rhombus structures are coupled with a cantilever to harvest energy from fluid motion and power the systems deep in an oil well with high pressure (200 MPa) and temperature (>160 °C). Fig. 18 (a) shows the flow-induced vibration will excite the cantilever and amplified by the Rhombus structure to act on the piezo as F'. Two water-resistant piezos are completely isolated from the fluid flow to reduce the corrosion and degradation effects. The maximum power generated is 25 mW across 100 Ω resistor at 20 L/min of flow rate and 305 Hz. The resonance frequency can be tuned by altering the beam's length and thickness. The piezo stack can ensure high fatigue limit and energy density [120].

A buckled-spring-mass bistable harvester implemented two Rhombus structures, flexure hinge, and mass blocks to capture the vibration energy as shown in

Fig. 18 (b). This architecture allows the energy of the dynamic mass to be transferred and amplified in the Rhombus. It exhibits wide bandwidth and a high power output of 16 mW under an acceleration of 3 m/s^2 at 26.5 Hz [121-123]. Besides, a spring-mass system is connected to a Rhombus structure inside a mounting frame with a total dimension of 16 × 29.1 × 65.5 mm^3. The impact force is induced onto the Rhombus PEH through the spring-mass system, typically through the collision between the sliding proof mass and spring limiter. This 2DOF system converts the ultra-low frequency human motion (<5 Hz) into high-frequency vibration (i.e. 2000 Hz of voltage response) and produces 0.93 mW of average power by strapping it below the knee while running [124].

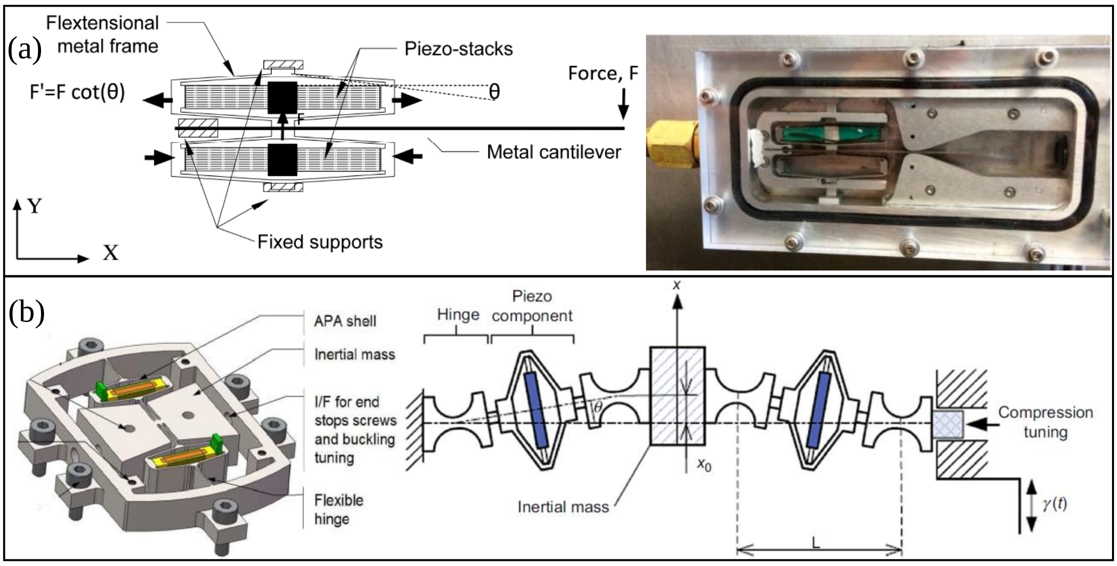

Fig. 18 (a) Combined structure of Rhombus and cantilever PEH in internal fluid flow (reproduced from [120]); (b) Buckled-spring-mass (BSM) bistable harvester (reproduced from [123])

4.6 Hybrid Rhombus Structure

A Hybrid Piezoelectric Energy Harvesting Transducer (HYPEHT) is designed with an outlook of Rhombus shape with one 33-mode Straight Inner Piezoelectric Multilayer Stack (SIPMS) at the middle and sandwiched by two 33-mode Curved Outer Piezoelectric Multilayer Stacks (COPMSs) as shown in Fig. 19 (a) [125]. The piezoelectric multilayer-stacked hybrid actuation/transduction system (stacked-HYBATS) has a different stacking axis of SIPMS which works in 31-mode as shown in Fig. 19 (b). It yielded 200% and 15% larger displacement than 31- and 33-mode Rhombus transducers [126].

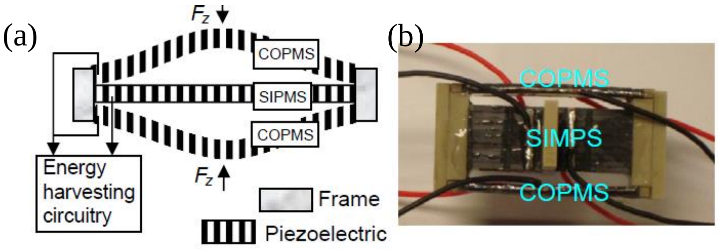

Fig. 19 (a) The HYPEHT with three 33-mode PZT stacks; (b) The stacked-HYBATS prototype with one 31-mode SIMPS and two 33-mode COMPSs (reprinted from [15], Copyright 2016, with permission from Elsevier)

A 35.5 × 18 × 10 mm^3 HYPEHT prototype has yielded 19 times more electrical energy output than a same size 31-mode flextensional PEH and 100-1000 times more than a Bimorph PEH. Hence, the advantages of HYPEHT can be summarized as firstly, almost all mechanical energy is coupled into the PZT because minimal non-piezoelectric materials are involved in the design. More electrical charges are produced because of the Rhombus force amplification mechanism and the PZT stack. Lastly, the curved 33-mode COPMSs are relatively soft and have large bending motion which leads to high power output [15, 127].

4.7 Bridge

In the Bridge structure, two parallel horizontal hinges of different height have replaced the slanted hinges in the Rhombus structure as shown in Fig. 20 (a). The aligned hinges in the Rhombus structure perform better in reducing the maximal stress and withstand a larger force due to its higher stiffness [128]. However, this high stiffness may reduce the power output as less frame deformation and lower stress applied at the PZT. Double flexure arms are designed in a Compound Bridge structure to increase the relatively low stiffness as shown in Fig. 20 (b). Fig. 20 (c) shows the right-circular (fillet) hinge is adopted to reduce the stress concentration. The Bridge structure has a displacement amplification ratio of 12 and is widely applied in the actuator [129] if compared to the PEH since the excitation area of the Bridge is limited to use as a PEH.

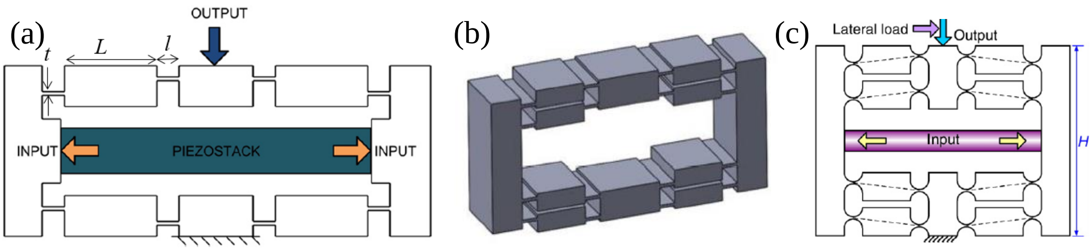

Fig. 20 (a) The displacement amplification mechanism of a Bridge piezoelectric actuator (reprinted from [130], Copyright 2015, with permission from Elsevier); (b) Compound Bridge structure with double flexure (double-beams) arms (reprinted from [131], Copyright 2018, with permission from Elsevier); (c) Additional filleted hinge design on the Compound Bridge actuator (reprinted from [129], Copyright 2011, with permission from Elsevier)

5. Flexcompressive Structure

5.1 33-mode Flexcompressive & Hull Structure

A compressive mode transducer is always preferred as the compressive mean normal stress is beneficial to retard the growth of cracks and increase the fatigue strength [132]. Flexcompressive or named as Compressive Flexure frame is developed to make the PEH directly work in compression mode as shown in Fig. 21 (a). This design has the advantage of eliminating the manufacturing complexity, the risks of buckling, and a large potential energy loss. It shows an 8 times greater voltage output and 112 times greater power output compared to a standalone PZT stack [133]. A two-beam compound Flexcompressive structure is developed to improve force stability of the harvester and applied in a backpack application [134].

Fig. 21 (b) presents another flexcompressive structure, which is named as the compressive Hull structure. It is developed with an inverted cavity shape from the flextensional Cymbal structure and has a larger loading area than the Flexcompressive structure. It shows 5 times greater voltage output than the Cymbal structure under the same boundary conditions due to its higher amplification effect [135].

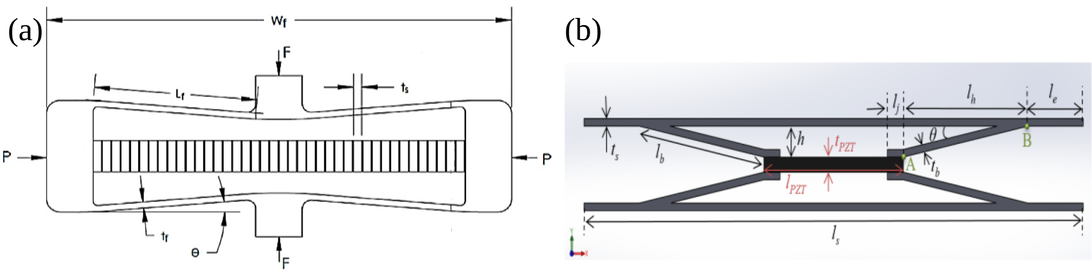

Fig. 21 (a) 33-mode stacked-PZT Flexcompressive structure (reprinted from [136], Copyright 2019, with permission from Elsevier); (b) Hull structure with its parameters (reprinted from [135], with permission from IOP)

Another study was carried out to investigate the effect of each parameter on the amplification factor of the Flexcompressive structure, such as the tilt angle, the thickness, and the length of the linkage: θ, $t_{linkage}$, and $l_{linkage}$; the thickness, the height, and the elastic modulus of the frame: t_{frame}, h_{frame}, and E_{frame}; as well as the width of the side block, t_{block}. The force amplification ratio will increase with longer and thinner linkages, thicker and shorter side blocks, smaller frame width, or soft frame materials. The thinner, narrower, and longer linkage will enhance its bending deflection causes a larger displacement and contraction of the PZT [137].

The force amplification ratio of Flexcompressive structure, k_{amp} has been presented in Eq. (13) which considered the nonlinear properties and deformation of the frame. Another two types of flexcompressional frames are compared with the original structure. Frame I is designed to have longer flexure linkages which enhance the bending deflection and two extended clamping sides for the PZT, while Frame II is larger and consists of two PZT stacks. The two frames have amplification ratios of

8.0 and 8.4, which are higher than the original frame with 3.5 ratio [137]. Frame I is then applied to harvest energy from foot strike [138].

$$k_{amp} = \frac{F_{out}}{F_{in}} = \frac{n_1 - n_2}{d_1 + d_2 + d_3 + d_4} \tag{13}$$

where

$n_1 = L_{linkage}^3 \cos\theta \sin\theta E_{frame}^2 A_{linkage} E_{stack} A_{stack} I_{block}$,

$n_2 = 12 L_{linkage} \cos\theta \sin\theta E_{frame}^2 I_{linkage} E_{stack} A_{stack} I_{block}$,

$d_1 = L_{linkage}^3 \sin^2\theta E_{frame}^2 A_{linkage} E_{stack} A_{stack} I_{block}$,

$d_2 = 12 L_{linkage} \cos^2\theta E_{frame}^2 I_{linkage} E_{stack} A_{stack} I_{block}$,

$d_3 = 12 L_{stack} E_{frame}^3 I_{linkage} A_{linkage} I_{block}$, and

$d_4 = 4 L_{block}^3 E_{frame}^2 I_{linkage} A_{linkage} E_{stack} A_{stack}$.

Another mathematics model of the amplification factor, α has been presented and equals to 8 by considering the frame geometry and the stiffness of the PZT stack, *k* as shown in Eq. (14). However, it decreases with increasing frequency, which is only 5.1 at 20 Hz as it does not consider the dynamic effects of the structure [139]. Hence, the developed PEH suitable for low-frequency energy harvesting such as from human walking as shown in Fig. 22. Since α is influenced by *k*, the optimization of the frame and PZT stack must be conducted concurrently [112, 136]. The optimal dimensions and amplification ratio of the PEH vary based on the type and amplitude of the input force. For example, with the optimized PZT stack parameters, such as the diameter, thickness, and number of PZT layer, an increase in power output by a factor of 21 is achieved, from 2.61 mW to 54.8 mW under walking condition. A factor of 9 is obtained under jogging condition, from 16.4 mW to 147 mW with the same PZT stack length. In practical, the PEH should be tested based on the worst-case loading condition, where the optimized stack under jogging condition is subjected to a walking input. This causes a 28% reduction in the average power output, end up with 39.1 mW [136].

$$\left(\frac{1}{k}+\frac{L\cos^2\theta}{2E_bA_b}+\frac{L^3\sin^2\theta}{12E_bI}\right)\alpha^2+\left(\frac{L\sin\theta\cos\theta}{E_bA_b}-(1-\tan\theta)\frac{L^3\sin\theta\cos\theta}{12E_bI}\right)\alpha+\frac{L\sin^2\theta}{2E_bA_b}-\frac{L^3\cos^2\theta\tan\theta}{12E_bI}=0 \tag{14}$$

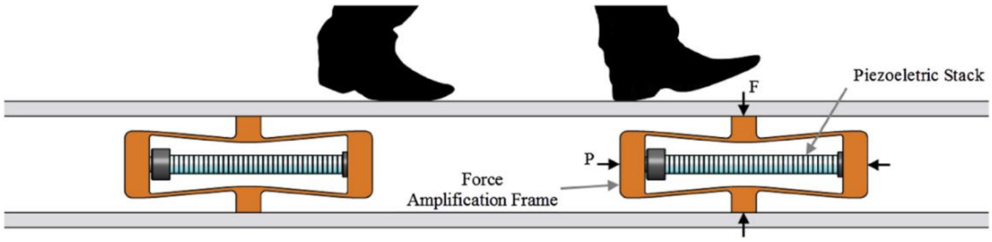

Fig. 22 Energy harvesting with Flexcompressive structure from human walking (reprinted from [136], Copyright 2011, with permission from Elsevier)

5.2 Flexcompressive with Hinge

Hinge with fillet design is added in a Flexcompressive frame to release the bending constraints between the thick beams and the blocks as shown in Fig. 23 (a). Stack holders are designed to hold the PZT stack in dynamic environment. The force amplification factor is found to be 8.5. The shoe with fewer PEH can generate more power due to larger force input to each structure. Six Flexcompressive PEHs in a shoe produce the highest power (14 mW, which is 56% more than that with eight PEHs) if compared to four and eight PEHs [140]. Another study applied the hinge design to reduce the energy stored in the inclined beams. Pre-stress is added by having a smaller cavity length for the PZT as shown in Fig. 23 (b) - (d). The load resistance should match with the internal impedance to obtain the maximum power generation.

The FEA displacement ratio of the PEH is 10.13, which is close to the experimental value of 9.50 [141].

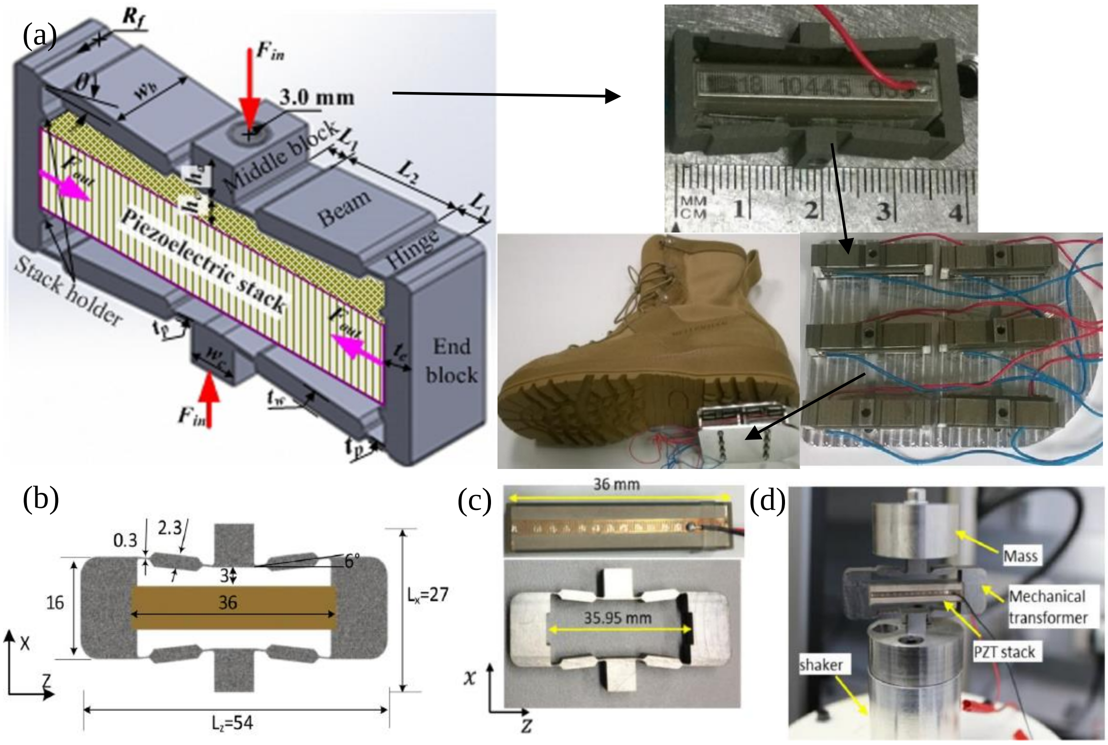

Fig. 23 (a) A Flexcompressive frame with hinges PEH that fixed into a boot (reprinted from [140], Copyright 2018, with permission from Elsevier); (b) Dimensions of the PEH: unit in mm, (c) the fabricated Flexcompressive structure with shorter cavity length than the PZT, and (d) experiment set up of the pre-stressed PEH with a proof mass (reprinted from [141], Copyright 2020, with permission from Elsevier)

Wang, Chen [133] shifted the hinge to the end block and increased the beam thickness. Experiments show that the Flexcompressive structure without hinge design has 8 times greater voltage output and 112 times greater power output than a standalone PZT stack. However, the PEH with hinge design is only 3 times and 17 times more than that of the standalone PZT stack because the flexure-induced increase in input energy is not sufficient to compensate for the potential energy loss stored in the flexures hinge even with the thicker beams. Hence, this type of hinge has poor energy converting efficiency.

6. Multistage Structure

6.1 Multistage Rhombus Structure

A two-stage force amplification mechanism was introduced with a larger vertical Rhombus structure and three horizontal smaller Rhombus frames inside as shown in Fig. 24 (a). Since the first stage output ends are connected to the input ends of the second stage frame, it is considered as a two-stage amplification mechanism that can capture more energy into the PZT [15, 142]. A multistage force amplification mechanism that involves three-stage Rhombus structure was employed by [143] to increase the effective piezoelectric constant and optimize the mechanical impedance match with increasing mechanical energy input.

Rhombus with hinge structure has been used as the second layer amplifier as shown in Fig. 24 (b) [8]. Wen and Xu [144] utilized two Rhombus frames (one inner and one outer) to obtain a large amplification ratio in compressive mode. They investigate the effect of hinges orientation on the Rhombus structure as shown in Fig. 24 (c) - (e). The original linkage design shares the stress evenly and reduces the risk of damage; whereas the aligned hinge and parallel hinge can reduce the stiffness of the frame. The original linkage design is selected by considering the safety factor, force amplification, and size of PEH. Based on the principle of energy conservation, the input energy is equal to the sum of output energy and stored strain energy in the frame. The unconverted stored strain energy can protect the structures from damage. Hence, a compromise between these two kinds of energy is the key to maintain an optimal force amplification ratio and safety factor. This two-stage Rhombus amplifier has a large force amplification ratio of 26 (even it is less than expected as the single outer and inner frames have amplification ratio of 9.54 and 8.88 respectively) and a compact size which is suitable for footstep PEH.

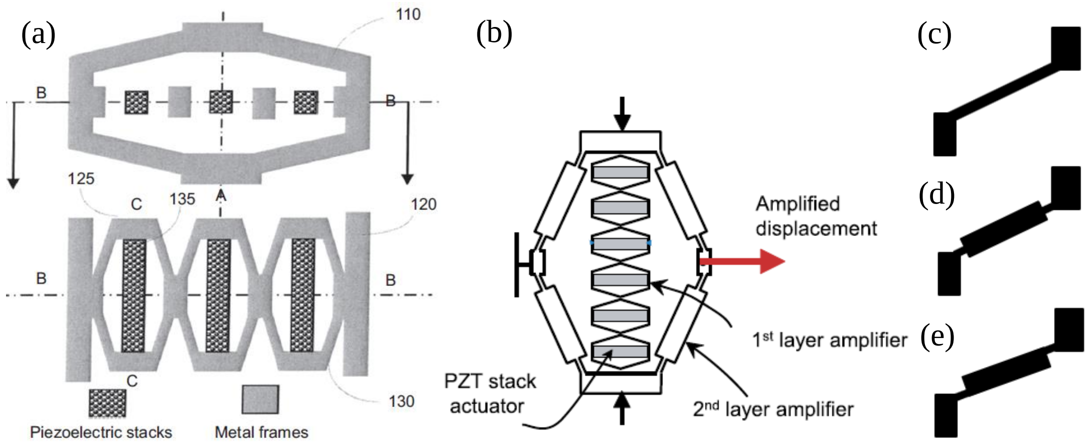

Fig. 24 Multistage Rhombus structure (a) The inner and outer frames lay in the perpendicular planes (reprinted from [15], Copyright 2016, with permission from Elsevier); (b) Both the inner and outer frames lay in the same plane (reprinted from [8], Copyright 2017, with permission from Elsevier); (c) Original design; (d) Aligned hinge; (e) Parallel hinge

Double flexure arm compound Rhombus frames are applied to achieve higher stiffness and safety factor (1.23 rises to 2.94) with a little scarification on the amplification ratio (22.62 reduces to 17.90). The total force amplification ratio, N is the multiplication of the inner and outer structure's amplification factors where $N = \eta N_{outer\ frame} N_{inner\ frame}$. The force transmission coefficient, η is equaled to 0.85, which is calculated from the FEA amplification factors, i.e. 17.9/(4.74 × 4.33). The maximum power of the PEH is 203 times over the standalone PZT stack [115].

6.2 Multistage Flexcompressive Structure

Wang, Chen [145] used three Flexcompressive structures with hinge design as the inner frame and one larger Flexcompressive structure as the outer frame to avoid the potential buckling failure in compression loading. Since there is strain energy stored in the frame, the magnification effect should consider both the force amplification ratio and the energy transmission efficiency (ratio of strain energy in the PZT and the total strain energy in the whole PEH). The two-stage Flexcompressive PEH has demonstrated a total of 20.8 times force amplification ratio and 18% energy transmission ratio, where 7.8 times force amplification and 24% energy transmission ratio are contributed by the inner frame, the rest is contributed by the outer frame. The power density is 127 times more than a standalone PZT stack.

Qian, Xu [146] then applied the two-stage Flexcompressive amplifier in a shoe heel to achieve autonomous power supply for wearable sensors and low-power electronics as shown in Fig. 25. The two-stage force amplification frames magnify the dynamic forces and transfer to the PZT stacks with minimum energy loss. The actual force amplification factor is found less than the simulated value of 12.8 and decreases with the increment of the loading force. This is due to the change in tilt angles of the beams and the stiffness of the PEH is not linear at large deformations. Hence, the analytical model is not accurate if it does not consider the large deformation and nonlinearity.

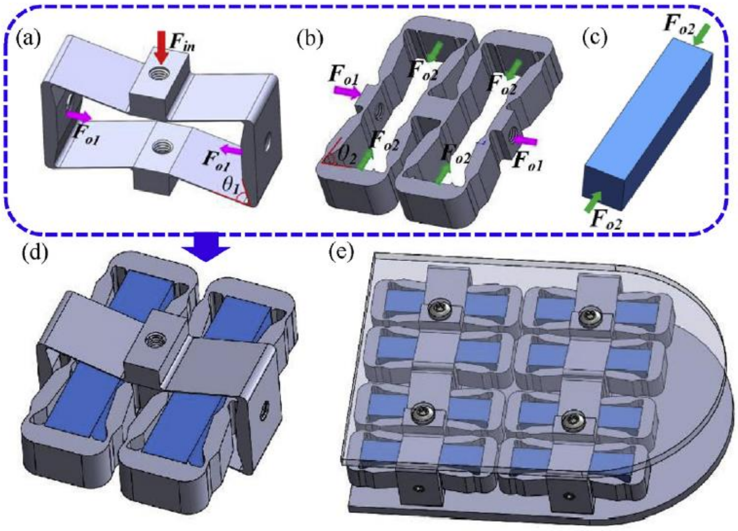

Fig. 25 (a) Flexcompressive outer frame; (b) Two series-connected Flexcompressive structures with hinge design as inner frame; (c) d33 PZT stack; (d) Two-stage Flexcompressive structure; (e) Configuration of the PEH in a shoe heel (reprinted from [146], Copyright 2019, with permission from Elsevier)

The two-stage compound Flexcompressive structure has a lower safety factor of 1.57 and an amplification ratio of 10.07 if compared to the two-stage compound Rhombus structure (2.98 and 15.21). This is because the amplified input force in the outer Flexcompressive structure reduces the output displacement and limits the amplification factor of the inner frame due to the law of conservation of energy [115].

6.3 Integrated Multistage Amplifier

Wen and Xu [147] introduced an underground integrated four-stage PEH to scavenge energy from human footsteps using a wedge mechanism, leverage mechanism, Flexcompressive structure, and Rhombus structure. The vertical input motion of the top plate is converted by the wedges to an amplified horizontal output motion. A larger forcing area is provided by having a top plate to withstand a larger load safely. Fig. 26 (a) - (c) show another integrated MAS which consists of a piezoelectric frame (PF) that composes of multiple piezoelectric beams and an amplification frame (AF) composes of a Rhombus-shaped link mechanism. It can easily achieve resonance conditions for low frequency excitations and has higher energy harvesting efficiency than the cantilever structure with the same volume of piezo material [148].

Wu and Xu [149] introduced a PEH which utilized the bidirectional friction force produced between footstep and harvester. A Rhombus structure is combined with a selectivity lever (SL) which composed of a lever mechanism and position limiters to utilize both pull and push inputs as shown in Fig. 26 (d) and (e). The lever mechanism is adopted to change the direction of input force, and position limiters are employed to distinguish between pull and push inputs. The FEA force amplification ratios are 12.20 and 13.14 under the pull and push input, respectively. The maximum average output power is 128.51 μW under back-and-forth input, which is 313.44 times higher than the PZT alone.

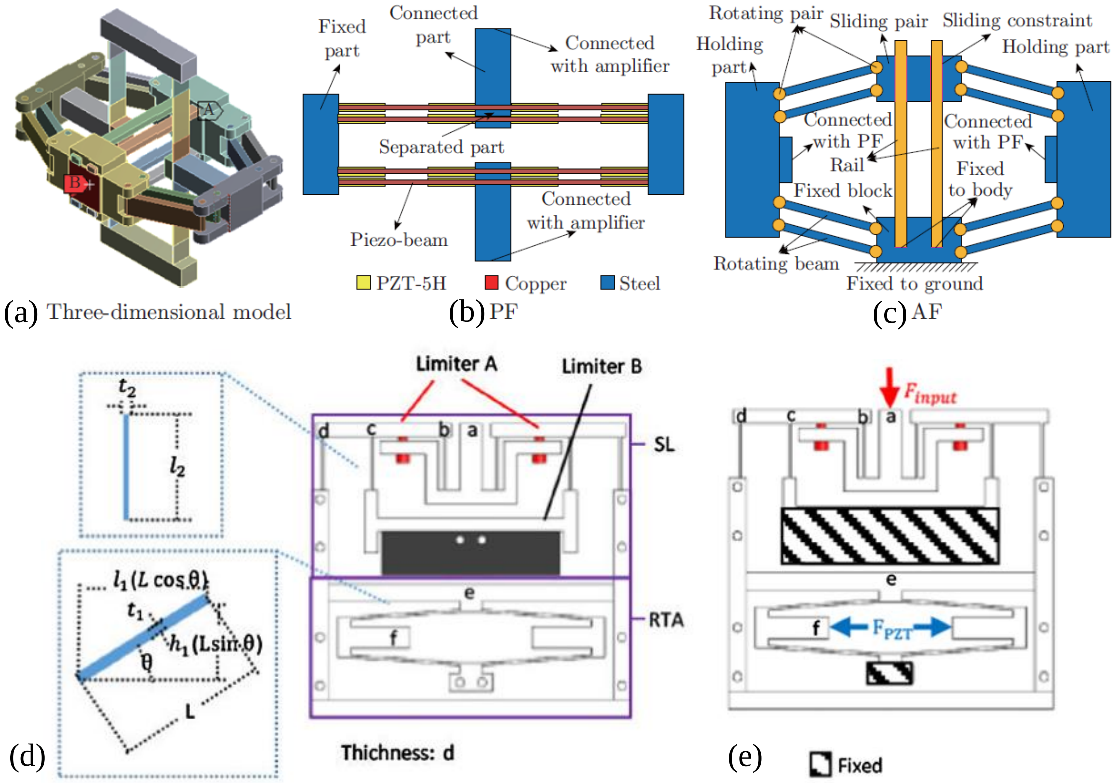

Fig. 26 (a) - (c) Integrated structure with Rhombus-shaped link mechanism (reprinted from [148], Copyright 2021, with permission from Springer), (d) Two-stage bidirectional Rhombus structure PEH and (e) the schematic mechanism under push input (reprinted from [149], Copyright 2019, with permission from Elsevier)

7. Comparison

In this section, the energy harvesting performance and the amplification ratio of MAS have been compared and discussed. Table 1 summarizes the excitation force, type of piezo, dimensions, output power, output voltage, optimum resistance, and application of different structures PEH described herein. A summary of the amplification factor based on the analytical theory has been presented in Table 2.

Direct comparison on the power output of PEHs has been made to evaluate their energy harvesting performance. However, the high power output may be due to a larger piezo used in the PEH. Hence, it is fair to compare the PEH with the calculated power density per unit of volume of piezo. Fig. 27 shows the power output and the calculated power density of each type of PEH under 0 - 2500 Hz. In order to mitigate the effect of piezo quality on the power density, a meticulous comparison is presented for PEHs that use the same piezo (same material properties), as denoted by circles in Fig. 27. It is noted that most of the PEH work under 200 Hz of excitation frequency to match with the vibration-based energy sources available in our surrounding. For instance, the commercial and industrial machines have around 120 Hz of vibration source, HVAC vents are around 60 Hz while human body movements, roadway pavement, bridge, and railways are <10 Hz [150].

Fig. 27 shows that the cantilever structure is widely tuned and utilized under the frequency of 20 - 80 Hz. The Cymbal PEH is comparatively more flexible to be designed under various frequencies among all the structure, whereas the Rhombus, Flexcompressive, and multistage structures focus on low-frequency vibration source which is below 10 Hz. Since the power harvesting from footsteps occurs at a very low frequency which is close to 1 Hz [151], many flexure structures show their implementation potential in this application. Moreover, the standalone PZT stack shows a capability to work under extremely high excitation frequency, around 2500 Hz.

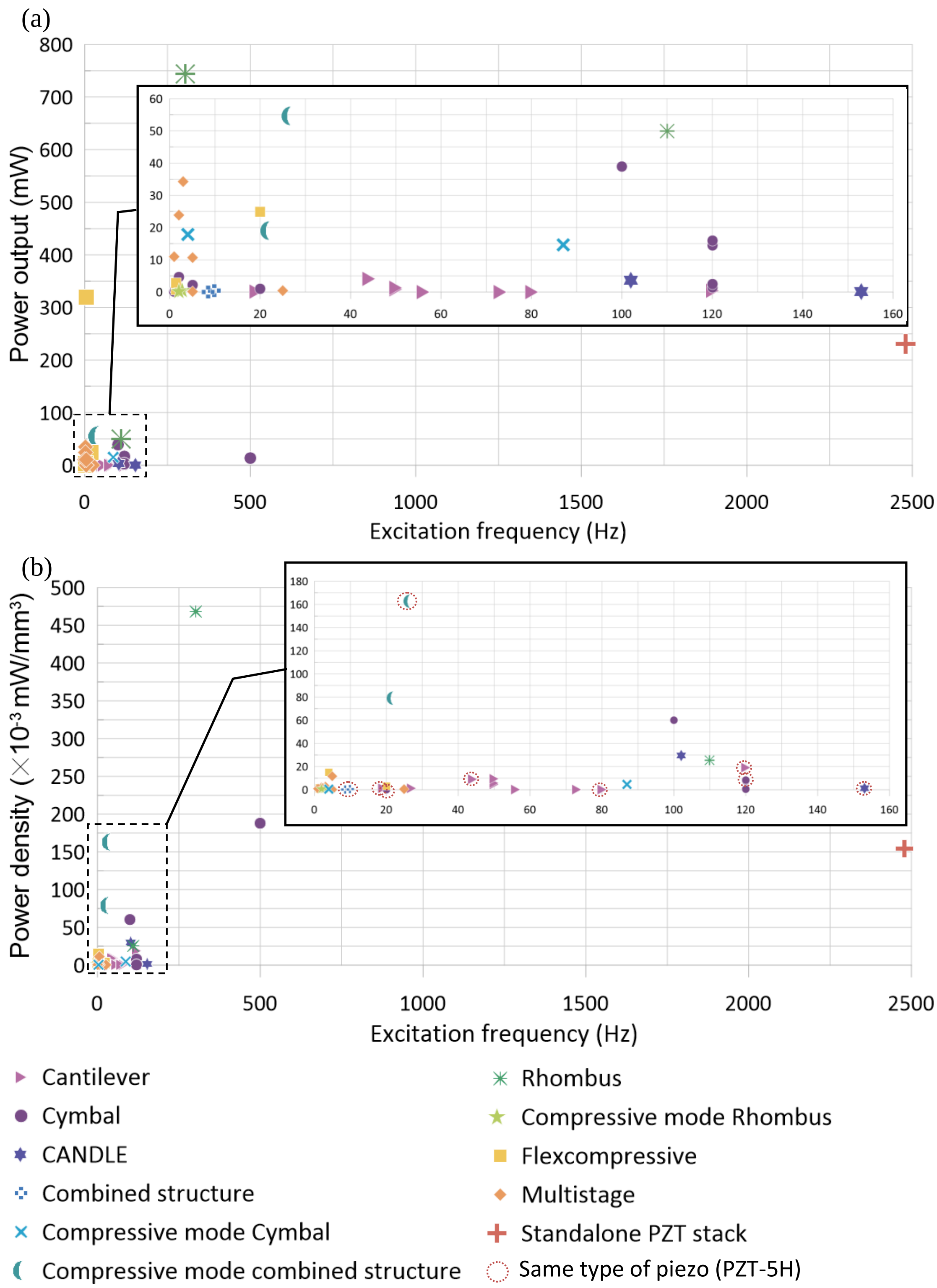

Fig. 27 Graph of (a) power output and (b) power density against the excitation frequency for different types of MAS of the PEH

Other than the excitation frequency, the applied force and electronics used on the PEH should be aware when comparing the power level of different PEHs [95]. Fig. 28 (a) presents the plot of power density by the excitation frequency and the applied force. Fig. 28 (b) shows that the PEH is designed to have greater power output by either targeting the higher frequency vibration source through the cantilever structure or the higher loading environment through the hybrid flexure type MAS. Hence, most of the MAS covered in this study, except for the cantilever, is designed and tested under higher loading force. Closer views with less overlapping points for the Cymbal and multistage structures are shown in Fig. 28 (d) and (e). The multistage structure is the recent trend that is frequently implemented in low frequency but high loading force environments due to its high durability and amplification factor, while the Cymbal is the most commonly applied structure over the decades.

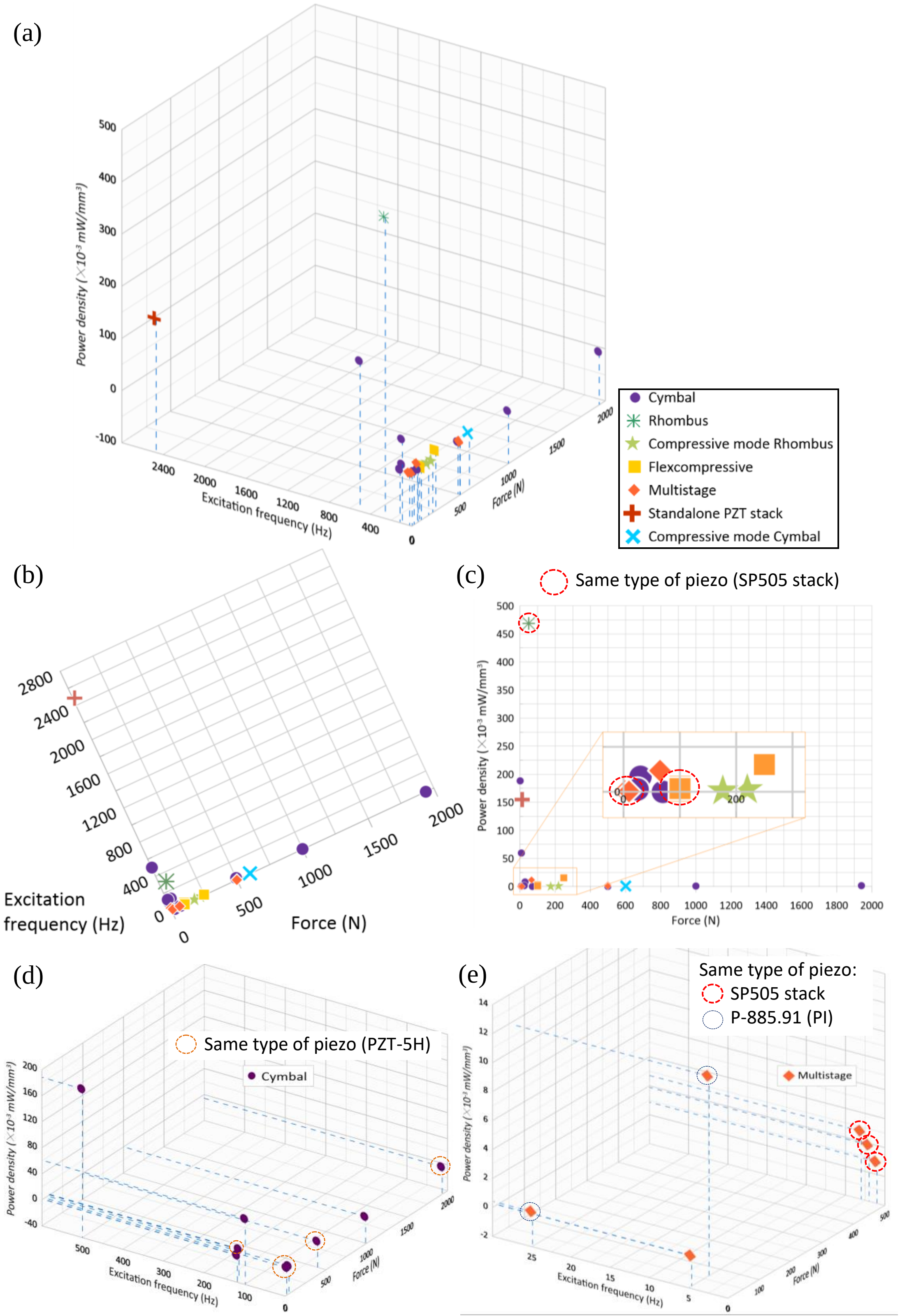

Fig. 28 (a) 3D plot of power density with the excitation frequency and the applied force for various PEHs with (b) the corresponding xy-plane, (c) and yz-plane; (d) The 3D plots for Cymbal structure and (e) multistage structure

Fig. 29 presents the power density of PEH under the acceleration source of less than 3 *g*. The cantilever structures show a comparatively low power density

(<0.02 mW/mm^3) as they are excited under a low vibration amplitude and medium range of frequency. This is because the cantilever robustness is insufficient to withstand higher cyclic force and stress. Hence, the combined cantilever and flextensional structures have higher power density as they utilize the high force amplification factor and robustness of flextensional structure to increase the load capacity in the high force environment. Meanwhile, the combined cantilever MAS could maintain the broadband working frequency characteristic of the cantilever structure in the combined MAS design, which highly increases its potential in different applications.

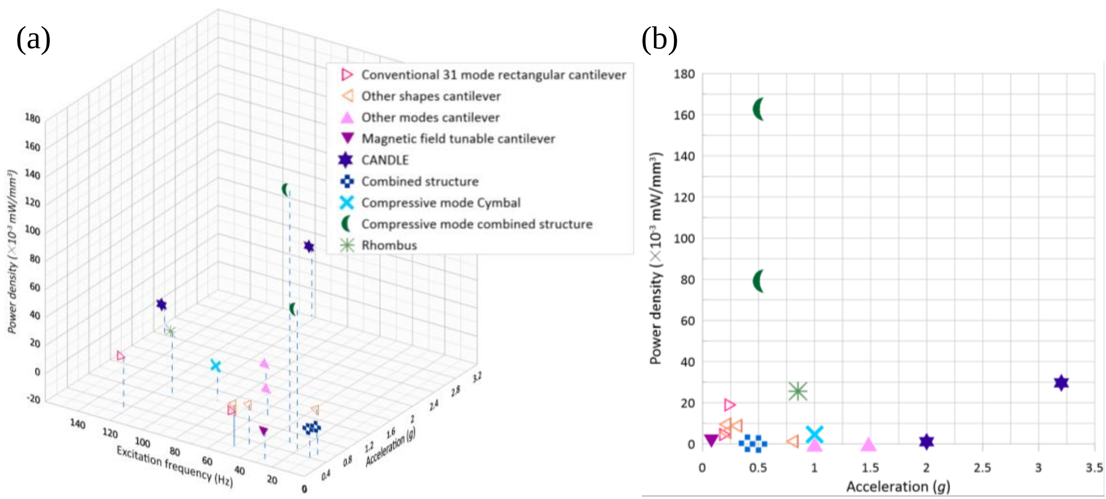

Fig. 29 (a) 3D plot of power density with the excitation frequency and the acceleration for various PEHs and (b) the corresponding yz-plane

Table 2 summarizes the equation of amplification ratio, the variable and theory used, the analytical, FEM, and experimental amplification ratio for different structures PEH. The elastic beam theorem and kinematic analysis on the flexure arm are the basic theory to apply in the model. It is noticed that the force amplification ratio has been up to 20 by using the multistage structure in a PEH, whereas a 112 power amplification ratio has been achieved using a Flexcompressive structure. A maximum of 12 displacement amplification ratio has been obtained experimentally with a Bridge or Rhombus structure. Generally, the displacement amplification ratio is slightly greater than the force amplification ratio (as shown in the Rhombus structure), while the amplification ratio which is calculated based on the power variable has the greatest value among all. In other words, an amplifier structure will have a different scale of increment in these variables even under the same input condition.

Thus, it is unfair to directly compare based on the value of the measured amplification ratio for different MAS. This is because the amplification ratio is computed based on different input and output variables for different studies, such as power, voltage, force, displacement, and energy. Furthermore, various theories have been used and different constraints have been considered when generating the analytical equation for the amplification ratio. Hence, the comparison should be made using the same variable under similar constraints.

Table 1 A summary of the performance based on the power output for various PEH structures

Amplifier structure	PZT material	Dimension of PZT (mm)	Loading force/Pressure/ Acceleration	Freq. (Hz)	Avg. Power (mW)	Power density ($\times 10^{-3}$ mW/mm^3)	Voltage (V)	Load (Ω)	Application [reference]
Rectangular cantilever	PZT-5H (Piezo Systems Inc.)	(11 × 3.2 × 0.28) × 2 pieces	0.25*g*	120	0.38	19.3*	14	250k	Vibration-based PEH (VPEH) for radio transmitter [32]
Triangular cantilever	PZT-5H	Trapezoid: w_{root} = 20, w_{tip} = 10, l = 10, t = 0.07	0.8mm displacemnet	80	0.0015	0.14*	1	333k	VPEH [37]
Rectangular cantilever	PSI-5A4E PZT (Piezo Systems Inc.)	(25 × 14 × 0.2) × 2 pieces	FEA: 0.2*g*; 10g proof mass	50	0.63*	4.5	54	Open circuit	VPEH [43]
Tapered cantilever		(w_{root} = 20.2, w_{tip} = 6.7, l = 26, t = 0.2) × 2 pieces			0.78*	5.6	60.3		
Reverse tapered cantilever		(w_{root} = 7, w_{tip} = 23.8, l = 22.7, t = 0.2) × 2 pieces			1.34*	9.6	72.6		
Zigzag cantilever	PZT-5H	45 × 15 × 0.2	0.8*g*	19	0.18 (peak)	1.33*	16 (peak)	10k	VPEH for wireless switch [48]
Arc-shaped PZT cantilever	PZT-5H	Arc-shaped: ($Ø_{outer}$ = 20, $Ø_{inner}$ = 19.5, w = 15, t = 0.5) × 2 pieces	0.3*g*	44	4.08	8.88*	29 (peak-to-peak)	100k	PEH [52]
Standalone PZT stack	PZT d33 stack: Navy Type II Ceram Tec SP505 (SP505 stack)	1 stack: 300 PZT layers = 7 × 7 × 32.3	$11.6N_{rms}$ (resonance mode)	2479	231	154.5	$2.9V_{rms}$	1M	[54]
			$40.0N_{rms}$ (off-resonance mode)	680	18.7	11.8	-	1M	
Barbell-shaped cantilever	d33 $BiScO_3$-$PbTiO_3$ ceramic	1 ring stack: $Ø_{outer}$ = 21, $Ø_{inner}$ = 8, t = 20	1*g*	56	0.0048	0.0008*	8	2.1M	High temperature VPEH [56]
Rectangular cantilever	d15 PZT-51 (Baoding HengSheng Acoustics Electron Apparatus Co. Ltd Baoding)	(13.0 × 2.5 × 1.0) × 2 pieces	1.48*g*	73	0.0087	0.13*	12.4 (peak-to-peak)	2.2M	[57]
Magnetic field tunable cantilever	PZT (APC International Ltd)	(34 × 20 × 0.16) × 2 pieces	0.08*g*	22-32	0.24-0.28	1.19*	-	26k	VPEH [58]
Moonie	PZT-5H	Ø = 32, t = 2	FEA: 0.7MPa	-	0.012mJ	-	44.9	-	[20]
Cymbal					0.489mJ		284.2		
Cymbal	D210 PZT (Dongil Technology, Korea)	Ø = 29, t = 1	7.8N	100	39	60	-	400k	VPEH [19]
	Noliac NCE51 and PiCeramics PIC 141	Ø = 30, t = 1	0.9MPa	-	0.016	0.023*	-	1M	Roadway PEH [84]
	PZT -5A	Ø = 35, t = 4	8.15N	120	1.40	0.36*	-	410k	VPEH [86]
	Radially layered PZT-5H (d31)	$Ø_{outer,1}$ = 50, $Ø_{inner,1}$ = 40, $Ø_{outer,2}$ = 30, $Ø_{inner,2}$ = 20, t	500N	20	0.92	0.17*	52.8 (open circuit,	0.8M	Roadway PEH [82]

		= 5					100MΩ)		
Cymbal with Unimorph	PZT-5H	Ø ≈ 25, t = 0.191	1940N	1	0.12	1.29*	-	3.3M	Underfloor/Roadway PEH [88]
Slotted Cymbal (18-fringe)	PZT-5H	Ø = 35, t = 2	30N	120	14.5	7.54*	85	520k	[85]
Slotted Cymbal (18-cone)					16	8.32*	90	500k	
Slotted Cymbal (circumferential)	PZT -5A	Ø = 35, t = 4	8.15N	120	2.5	0.65*	-	400k	VPEH [86]
Rectangular Cymbal	PMN-PT single crystal $0.71Pb(Mg_{1/3}Nb_{2/3})O_3$-$0.29PbTiO_3$	26.6 × 4 × 0.7	0.55N	500	14	188	45.7 (peak)	74k	VPEH [152]
Rectangular Cymbal	PZT-5H	32 × 32 × 2	0.7MPa	-	1.13mJ	-	FEA: 382.0	-	[20]
				1	-		168.8		
Rectangular Cymbal		30 × 20 × 2	0.7MPa	10	-	-	168.8	-	[93]
Arc Rectangular Cymbal					-		230		
Arch Rectangular Cymbal					0.6mJ		286		
Arch Rectangular Cymbal			0.75MPa @2.5m/s	-	-	-	202	-	Roadway PEH [94]
Arch Circular Cymbal	PZT-5H (Morgan Electro Ceramics)	Ø = 3, t = 0.5	24.8N	1.19	0.66	1.37	82 (peak)	2.6M	Footstep PEH [95]
Rectangular Cymbal (dual substrates)	DL-53HD PZT (Del Piezo Specialities)	52 × 30 × 4	1kN	2	4.68	0.75*	-	6.6M	Shoes PEH [9]
			4.8km/h	1.4	2.5	0.40*	180 (peak)	2M	
Rectangular Cymbal	PZT-5X d33 stack (Sinocera, State College, PA)	1 stack: 7 PZT layers = 32 × 32 × 2	0.7MPa	-	0.74 mJ	-	556	Open circuit	Roadway PEH [80]
		64 stacks	70kPa	5	2.1	0.0023*	-	400k	
CANDLE (Rectangular Cymbal)	PMNT (0.71PMN-0.29PT)	25 × 5 × 1	3.2g	102	3.7	29.6	38 (peak)	251k	VPEH [98]
CANDLE (Circular Cymbal)	PZT-5H d31 stack	(Ø = 12.7; t = 0.5) × 2 disks	2g	153	0.14	1.12*	2.38	40k	VPEH [100]
Combined structure (3 Rectangular Cymbals & Cantilever with magnet stoppers)	PZT-5H (d31)	(40 × 10 × 0.8) × 3 pieces	0.4g	9.9	0.39 (peak)	0.40*	-	390k	VPEH [102]
			0.5g	8.5	0.03	0.03*			
Compressive mode Rectangular Cymbal	PZT-4 d33 ring stack	(1 stack: 10 PZT rings $Ø_{outer}$ = 15, $Ø_{inner}$ = 5, t = 10) × 2 stacks	1g	87	14.6	4.7*	111 (peak-to-peak)	40k	Footstep PEH [92]
	PZT d33 stack	(20 × 20 × 36) × 2 stacks	600N	4	17.8	0.62*	-	120k	[106]
Compressive mode combined structure (Rectangular Cymbal & cantilever)	PZT-5A	32 × 15 × 0.5	0.5g	21	19 (peak)	79.2*	-	300k	VPEH for WSN [10]
	PZT-5H	32 × 15 × 0.7	0.5g	25.7	54.7 (peak)	162.8	-	100k	VPEH [104]
Rhombus	PZT d33 stack: APA 400M-	2 stacks ≈ 40 × 7 × 7	0.85g	110	50	25.5*	-	2k	VPEH, Self-

	MD								powered AM transmitter [117]
	(SP505 stack)	32.4 × 7 × 7	50N	303	744*	468*	12.5	1M	[118]
Compressive mode Rhombus with hinges	PZT d33 stack	1 stack: 130 PZT layers = 16 × 5 × 5	220N	2.8	FEA: 0.4	1*	-	19.2k	Backpack PEH [116]
			176N	2	0.176	0.44*			
Flexcompressive	PZT d33 stack (P-113-00)	1 stack: 250 PZT layers Ø = 10, *l* = 42	53.6N (peak)	-	6.97 (peak)	2.11*	18.7 (peak)	70k	Shoes PEH [133]
	PZT-4 d33 ring stack	1 stack: 12 PZT rings $Ø_{outer}$ = 15, $Ø_{inner}$ = 8, *l* = 62	100N	20	24.9 (peak)	3.18*	240	2.3M	[139]
	PZT d33 ring stack	1 stack: Ø = 13, *l* = 160	250N	4	320	15.07*	17.9V_{rms}	1k	Underfloor PEH [136]
Flexcompressive	(SP505 stack)	32.34 × 7 × 7	100N	1.4	0.65 2.00 (peak)	0.41* 1.26* (peak)	-	50k	[137]
Flexcompressive with longer linkage					2.7 7.7 (peak)	1.70* 4.86* (peak)			
Flexcompressive with hinge		6 stacks	4.8km/h	-	FEA: 9.0	0.95*	5.8V_{rms}	3.6k	Shoes PEH [140]
					Exp: 8.5	0.89*	5.5V_{rms}		
Two-stage compound Rhombus	PZT d33 stack: P-885.91 (Physik Instrumente (PI) Co., Ltd.)	1 stack = 36 × 5 × 5	2.33N	25	0.34	0.38*	-	2k	Footstep PEH [115]
Two-stage Rhombus & lever	PZT d33 stack: RP150 Harbin Soluble Core Tech Co., Ltd.	1 stack = 28 × 5 × 5	10N (Push input)	5	0.067	0.096*	2.9 (peak-to-peak)	12k	[149]
			10N (Pull input)	5	0.055	0.079*	2.6	11k	
Two-stage Flexcompressive (1 outer, 3 inner frames)	(SP505 stack)	(32.34 × 7 × 7) × 3 stacks	100g proof mass	37	-	2642mW/g^2	-	1.722k	[145]
Two-stage Flexcompressive (4 structures: 1 outer, 2 inner frames)		8 stacks	500N (FEA)	3	34.3	2.71*	-	1.6k	Shoes PEH [146]
			500N	2	23.9	1.89*		2.4k	
			500N	1	11.0	0.87*		5.1k	
			4.8km/h	-	10.4	0.82*		-	
Four-stage Rhombus, Flexcompressive, wedge & lever	PZT d33 stack: P-885.91 (PI)	1 stack = 36 × 5 × 5	82.3N (one complete press-and-release cycle)	-	34.8 (peak)	38.7*	26.4	20k	Floor tile PEH [147]
			65N	5	10.6	11.8*	-	10k	

* denotes calculated value; *w* = width, *l* = length, *t* = thickness, Ø = diameter

Table 2 A summary of the amplification factor based on the analytical theory for various structures

Variable	Theory & equation	Amplification ratio				Reference
		Structure	Analytical	FEM	Experiment	
Energy	Energy transmission coefficient *refer Eq. (10)	Moonie	-	0.012	-	[20]
		Cymbal	-	0.015	-	
		Rectagular Cymbal	-	0.037	-	
Force	Kinematic principle $R = F_{output}/F_{input} = \cot\theta$	Rectagular Cymbal, Rhombus	Varies based on the inclined angle, θ	-	-	[9, 92, 110]
	$R_{total} = F_{output}/F_{input}$	4-beam compound Rhombus	-	3.9	-	[115]
		Two-stage compound Flexcompressive	-	10.1	-	
	Compatibility condition theorem *refer Eq. (13)	Flexcompressive	3.4	3.7	3.5	[137]
		Flexcompressive with longer linkage	8.1	8.2	8.0	
Force & voltage	Elastic beam theory $R_{total} = F_{output}/F_{input} = \eta \times R_{first\ stage} \times R_{second\ stage}$	Two-stage Rhombus	-	26	-	[144]
			-	22.6	-	[115]
		Two-stage compound Rhombus	-	17.9	17.5	[115]
	Kinematic principle for ideal case Theory: $R_{total} = R_{first\ stage} \times R_{second\ stage}$; $R = \cot\theta$ FEA: $R_{total} = F_{output}/F_{input}$ Experiment: Ratio of the gradients (from graph of output voltage against input force) for the developed PEH over the standalone PZT	Two-stage Flexcompressive (1 outer, 3 inner frames)	-	21	20.8	[145]
		Two-stage Flexcompressive (4 structures: 1 outer, 2 inner frames)	-	12.8	9.2@80N	[146]
					4.5@500N	
		Four-stage Rhombus, Flexcompressive, wedge & lever	-	18.8	17.9	[147]
			13.1@3.7˚	-	Deviation<10%	
Displacement	Beam theory and kinematic analysis *refer Eq. (11)	Rhombus	9.5	6.2	-	[111]
	Kinematic principle and elastic beam theory *refer Eq. (12)	Rhombus	9@3.2˚	8@3.2˚	-	[112]
			13.1@3.7˚	-	Deviation<10%	
	$R_{amo} = \Delta y_{output}/\Delta x_{input}$	Rhombus with hinge	9	9	Deviation<7%	[113]
			-	10.9	-	[116]
		Bridge	12.8	11.9	12.4	[153]
	Kinematic principle and elastic mechanism $R_{amo} = (l_a \cos\alpha)/[\cos\alpha\,(t^2 \cos\alpha / 6\, l_a \sin\alpha) + l_a \sin\alpha]$	Rhombus/ Bridge	44@0.8˚	19@1.3˚	-	[110]
			18.8	15.4	12.0	[130]
Power	$R_{amo} = P_{developed\ PEH}/P_{standalone\ PZT}$	Flexcompressive	-	-	112	[133]
Power & voltage	Elastic beam theory *refer Eq. (14)	Flexcompressive	8	8	52 (power) 7.2 (voltage)	[139]

8. Conclusion

The development of a high-efficiency PEH is essential to provide sufficient power for self-powered IoT devices or WSN in remote places. Optimization on the MAS has been done to further improve the efficiency of the transducer in terms of force amplification ratio or power output. This work summarizes the working principle, application, performance, and characteristics, especially the advantages and disadvantages of different MAS. Meanwhile, it provides significant insight and suggestions on the future trend and potential implementation of MAS in different application scenarios to improve the efficiency of PEH.

The cantilever structure is capable for broadband energy harvesting from mechanical vibration source, but a higher flexibility piezo has to be used instead of PZT under high force environment due to its fragile characteristics. The piezo stacking design increases the load capacity and the power output by utilizing the 33-mode of piezo. The flexure structure has been widely developed as it has higher stiffness, load capacity, and amplification factor. The derivatives of flextensional structures should be implemented based on the applications, such as the compound beam will increase the stiffness of the structure, whereas the hinge design will mitigate the stagnation of bending mechanical energy in the frame. The fillet design will reduce stress concentration. A compressive mode PEH is always preferred due to the larger compressive yield strength of a piezo. Many designs have been proposed, such as fixing the piezo outside of the flextensional frame, applying a pulling force on the flextensional structure, or using a multistage flextensional frame to activate the compression mode in the piezo. However, it will lead to a bulky design and is impractical for those applications where pulling force is absent. Hence, the Flexcompressive structure has better overall performance as it utilizes the 33-mode parallel-connected piezo stack in a compact and direct compressive way. The combined structures have a wider bandwidth with the adopted cantilever structure, while the multistage structure can achieve a greater amplification effect which should be implemented in future design.

There are several ways to compare the efficiency of the MAS such as based on the force or displacement amplification ratio, voltage, or power density (per unit volume of piezo), and the electrical energy stored in the PEH. This article presents the figure of merit on the harvesting performance of PEH and a concise summary of the common and impactful MAS published in this area. It also summarizes the amplification ratio of each structure with the theory and variable used. Since the force amplitude and the excitation frequency used in the previous studies are all different, this review paper attempts to ease the comparison for future research with the summary. This is because the preferred MAS may vary depending on the forcing environment and application focus. In short, a constant evaluation factor must be used while comparing the MAS or PEH under the same forcing environment.

9. Disclosure Statement

The authors report there are no competing interests to declare.

10. Funding

The authors wish to acknowledge the financial support from Universiti Malaya International Collaboration Grant (ST046-2022) under SATU Joint Research Scheme Program; and Universiti Malaya Research University Grant (RU Faculty) under grant number GPF081A-2018.

References

[1] Li T, Lee PS. Piezoelectric Energy Harvesting Technology: From Materials, Structures, to Applications. Small Structures. 2022;3(3):2100128.

[2] Liu L, Guo X, Lee C. Promoting smart cities into the 5G era with multi-field Internet of Things (IoT) applications powered with advanced mechanical energy harvesters. Nano Energy. 2021;88:106304.

[3] Boisseau S, Despesse G, Seddik BA. Electrostatic conversion for vibration energy harvesting. Small-Scale Energy Harvesting. 2012:1-39.

[4] Wu N, Bao B, Wang Q. Review on engineering structural designs for efficient piezoelectric energy harvesting to obtain high power output. Engineering Structures. 2021;235:112068.

[5] Siang J, Lim MH, Salman Leong M. Review of vibration-based energy harvesting technology: Mechanism and architectural approach. International Journal of Energy Research. 2018;42(5):1866-93.

[6] Iqbal M, Malik Muhammad N, Khan F, Abas PE, Cheok Q, Iqbal A, et al. Vibration-based piezoelectric, electromagnetic, and hybrid energy harvesters for microsystems applications: A contributed review. International Journal of Energy Research. 2020;45:1-38.

[7] Zhang P. 1 - Sensors and Actuators for Industrial Control. In: Zhang P, editor. Industrial Control Technology. Norwich, NY: William Andrew Publishing; 2008. p. 1-186.

[8] Ueda J, Schultz JA, Asada HH. 1 - Structure of cellular actuators. In: Ueda J, Schultz JA, Asada HH, editors. Cellular Actuators: Butterworth-Heinemann; 2017. p. 1-44.

[9] Kuang Y, Daniels A, Zhu M. A sandwiched piezoelectric transducer with flex end-caps for energy harvesting in large force environments. Journal of Physics D: Applied Physics. 2017;50.

[10] Yang Z, Zu J. High-efficiency compressive-mode energy harvester enhanced by a multi-stage force amplification mechanism. Energy Conversion and Management. 2014;88:829-33.

[11] Kang G-d, Cao Y-m. Application and modification of poly (vinylidene fluoride)(PVDF) membranes–a review. Journal of membrane science. 2014;463:145-65.

[12] Yadav D, Yadav J, Vashistha R, Goyal DP, Chhabra D. Modeling and simulation of an open channel PEHF system for efficient PVDF energy harvesting. Mechanics of Advanced Materials and Structures. 2021;28(8):812-26.

[13] Yue R, Ramaraj SG, Liu H, Elamaran D, Elamaran V, Gupta V, et al. A review of flexible lead-free piezoelectric energy harvester. Journal of Alloys and Compounds. 2022;918:165653.

[14] Zhao H, Yu J, Ling J. Finite element analysis of Cymbal piezoelectric transducers for harvesting energy from asphalt pavement. Journal of the Ceramic Society of Japan. 2010;118:909-15.

[15] Xu TB. 7 - Energy harvesting using piezoelectric materials in aerospace structures. In: Yuan F-G, editor. Structural Health Monitoring (SHM) in Aerospace Structures: Woodhead Publishing; 2016. p. 175-212.

[16] Chen J, Qiu Q, Han Y, Lau D. Piezoelectric materials for sustainable building structures: Fundamentals and applications. Renewable and Sustainable Energy Reviews. 2019;101:14-25.

[17] M′boungui G, Adendorff K, Naidoo R, Jimoh AA, Okojie DE. A hybrid piezoelectric micro-power generator for use in low power applications. Renewable and Sustainable Energy Reviews. 2015;49:1136-44.

[18] Yang Z, Zhou S, Zu J, Inman D. High-performance piezoelectric energy harvesters and their applications. Joule. 2018;2(4):642-97.

[19] Kim HW, Batra A, Priya S, Uchino K, Markley D, Newnham RE, et al. Energy Harvesting Using a Piezoelectric "Cymbal" Transducer in Dynamic Environment. Japanese Journal of Applied Physics. 2004;43(9A):6178-83.

[20] Zhao H, Ling J, Yu J. A comparative analysis of piezoelectric transducers for harvesting energy from asphalt pavement. Journal of the Ceramic Society of Japan. 2012;120:317-23.

[21] Yang Z, Erturk A, Zu J. On the efficiency of piezoelectric energy harvesters. Extreme Mechanics Letters. 2017;15:26-37.

[22] Covaci C, Gontean A. Piezoelectric Energy Harvesting Solutions: A Review. Sensors. 2020;20(12):3512.

[23] Dal Bo L, Gardonio P. Energy harvesting with electromagnetic and piezoelectric seismic transducers: Unified theory and experimental validation. Journal of Sound and Vibration. 2018;433:385-424.

[24] Gardonio P, Dal Bo L. Scaling laws of electromagnetic and piezoelectric seismic vibration energy harvesters built from discrete components. Journal of Sound and Vibration. 2020;476:115290.

[25] Dash RC, Maiti DK, Singh BN. A finite element model to analyze the dynamic characteristics of galloping based piezoelectric energy harvester. Mechanics of Advanced Materials and Structures. 2022;29(25):4170-9.

[26] Dash RC, Maiti DK, Singh BN. Nonlinear dynamic analysis of galloping based piezoelectric energy harvester employing finite element method. Mechanics of Advanced Materials and Structures. 2022;29(26):4964-71.

[27] Li H, Tian C, Deng ZD. Energy harvesting from low frequency applications using piezoelectric materials. Applied physics reviews. 2014;1(4):041301.

[28] Gao X, Shih W-H, Shih WY. Vibration energy harvesting using piezoelectric unimorph cantilevers with unequal piezoelectric and nonpiezoelectric lengths. Applied Physics Letters. 2010;97(23).

[29] Panda SK, Srinivas J. Electro-structural analysis and optimization studies of laminated composite beam energy harvester. Mechanics of Advanced Materials and Structures. 2022;29(25):4193-205.

[30] Li L, Xu J, Liu J, Gao F. Recent progress on piezoelectric energy harvesting: structures and materials. Advanced Composites and Hybrid Materials. 2018;1(3):478-505.

[31] Aladwani A, Aldraihem O, Baz A. A Distributed Parameter Cantilevered Piezoelectric Energy Harvester with a Dynamic Magnifier. Mechanics of Advanced Materials and Structures. 2014;21(7):566-78.

[32] Roundy S, Wright PK. A piezoelectric vibration based generator for wireless electronics. Smart Materials and Structures. 2004;13(5):1131-42.

[33] Abdelkefi A, Najar F, Nayfeh AH, Ayed SB. An energy harvester using piezoelectric cantilever beams undergoing coupled bending–torsion vibrations. Smart Materials and Structures. 2011;20(11):115007.

[34] Mei J, Li L. Split-electrode piezoelectric scavengers for harvesting energy from torsional motions. Journal of Physics: Conference Series. 2013;476:012136.

[35] Hu G, Tang L, Das R, Marzocca P. A two-degree-of-freedom piezoelectric energy harvester with stoppers for achieving enhanced performance. International Journal of Mechanical Sciences. 2018;149:500-7.

[36] Keshmiri A, Deng X, Wu N. New energy harvester with embedded piezoelectric stacks. Composites Part B: Engineering. 2019;163:303-13.

[37] Glynne-Jones P, Beeby SP, White NM. Towards a piezoelectric vibration-powered microgenerator. IEE Proceedings - Science, Measurement and Technology. 2001;148(2):68-72.

[38] Raju SS, Umapathy M, Uma G. Design and analysis of high output piezoelectric energy harvester using non uniform beam. Mechanics of Advanced Materials and Structures. 2020;27(3):218-27.

[39] Roundy S, Leland ES, Baker J, Carleton E, Reilly E, Lai E, et al. Improving power output for vibration-based energy scavengers. IEEE Pervasive Computing. 2005;4(1):28-36.

[40] Chattaraj N, Ganguli R. Performance improvement of a piezoelectric bimorph actuator by tailoring geometry. Mechanics of Advanced Materials and Structures. 2018;25(10):829-35.

[41] Mateu L, Moll F. Optimum Piezoelectric Bending Beam Structures for Energy Harvesting using Shoe Inserts. Journal of Intelligent Material Systems and Structures. 2005;16.

[42] Dietl J, Garcia E. Beam Shape Optimization for Power Harvesting. Journal of Intelligent Material Systems and Structures - J INTEL MAT SYST STRUCT. 2010;21:633-46.

[43] Benasciutti D, Moro L, Zelenika S, Brusa E. Vibration energy scavenging via piezoelectric bimorphs of optimized shapes. Microsystem Technologies. 2009;16:657-68.

[44] Liu Y, Hu B, Cai Y, Zhou J, Liu W, Tovstopyat A, et al. Design and Performance of ScAlN/AlN Trapezoidal Cantilever-Based MEMS Piezoelectric Energy Harvesters. IEEE Transactions on Electron Devices. 2021;68(6):2971-6.

[45] Ben Ayed S, Abdelkefi A, Najar F, Hajj MR. Design and Performance of Variable Shaped Piezoelectric Energy Harvesters. Journal of Intelligent Material Systems and Structures. 2013;25.

[46] Keshmiri A, Wu N. Structural stability enhancement by nonlinear geometry design and piezoelectric layers. Journal of Vibration and Control. 2018;25(3):695-710.

[47] Kaur S, Graak P, Gupta A, Chhabra P, Kumar D, Shetty A. Effect of various shapes and materials on the generated power for piezoelectric energy harvesting system. AIP Conference Proceedings. 2016;1724(1):020076.

[48] Ma T, Chen N, Wu X, Du F, Ding Y. Investigation on the design and application of 3-dimensional wide-band piezoelectric energy harvester for low amplitude vibration sources. Smart Materials and Structures. 2019;28(10):105013.

[49] Wang J, Xue Z, Cai C, Wang D. A Novel Piezoelectric Energy Harvester With Different Circular Arc Spiral Cantilever Beam. IEEE Sensors Journal. 2022;22(11):11016-22.

[50] Zhou S, Chen W, Malakooti M, Cao J, Inman D. Design and modeling of a flexible longitudinal zigzag structure for enhanced vibration energy harvesting. Journal of Intelligent Material Systems and Structures. 2016;28.

[51] Li X, Yu K, Upadrashta D, Yang Y. Multi-branch sandwich piezoelectric energy harvester: mathematical modeling and validation. Smart Materials and Structures. 2019;28(3):035010.

[52] Yang Z, Wang YQ, Zuo L, Zu J. Introducing arc-shaped piezoelectric elements into energy harvesters. Energy Conversion and Management. 2017;148:260-6.

[53] Eghbali P, Younesian D, Farhangdoust S. Enhancement of piezoelectric vibration energy harvesting with auxetic boosters. International Journal of Energy Research. 2020;44(2):1179-90.

[54] Xu T-B, Siochi EJ, Kang JH, Zuo L, Zhou W, Tang X, et al., editors. A piezoelectric PZT ceramic multilayer stack for energy harvesting under dynamic forces. ASME 2011 International Design Engineering Technical Conferences and Computers and Information in Engineering Conference; 2011: Citeseer.

[55] Xu T-B, Siochi EJ, Kang JH, Zuo L, Zhou W, Tang X, et al. Energy harvesting using a PZT ceramic multilayer stack. Smart Materials and Structures. 2013;22(6):065015.

[56] Wu J, Chen X, Chu Z, Shi W, Yu Y, Dong S. A barbell-shaped high-temperature piezoelectric vibration energy harvester based on BiScO3-PbTiO3 ceramic. Applied Physics Letters. 2016;109(17):173901.

[57] Zhao J, Zheng X, Zhou L, Zhang Y, Sun J, Dong W, et al. Investigation of ad15mode PZT-51 piezoelectric energy harvester with a series connection structure. Smart Materials and Structures. 2012;21(10):105006.

[58] Challa VR, Prasad MG, Shi Y, Fisher FT. A vibration energy harvesting device with bidirectional resonance frequency tunability. Smart Material Structures. 2008;17:015035.

[59] Ibrahim DS, Beibei S, Oluseyi OA, Peng Z, Sharif U. Nonlinear dynamic analysis of a reciprocative magnetic coupling on performance of piezoelectric energy harvester interfaced with DC circuit. Mechanics of Advanced Materials and Structures. 2022;29(26):5488-500.

[60] Harne RL, Wang KW. A review of the recent research on vibration energy harvesting via bistable systems. Smart Materials and Structures. 2013;22(2):023001.

[61] Huang D, Zhou S, Litak G. Theoretical analysis of multi-stable energy harvesters with high-order stiffness terms. Communications in Nonlinear Science and Numerical Simulation. 2019;69:270-86.

[62] Sun S, Tse PW. Modeling of a horizontal asymmetric U-shaped vibration-based piezoelectric energy harvester (U-VPEH). Mechanical Systems and Signal Processing. 2019;114:467-85.

[63] Yang W, Towfighian S. A hybrid nonlinear vibration energy harvester. Mechanical Systems and Signal Processing. 2017;90:317-33.

[64] Erturk A, Hoffmann J, Inman DJ. A piezomagnetoelastic structure for broadband vibration energy harvesting. Applied Physics Letters. 2009;94(25):254102.

[65] Fan K, Tan Q, Liu H, Zhang Y, Cai M. Improved energy harvesting from low-frequency small vibrations through a monostable piezoelectric energy harvester. Mechanical Systems and Signal Processing. 2019;117:594-608.

[66] Zhou S, Cao J, Erturk A, Lin J. Enhanced broadband piezoelectric energy harvesting using rotatable magnets. Applied Physics Letters. 2013;102(17):173901.

[67] Man D, Xu G, Xu H, Xu D, Tang L. Nonlinear Dynamic Analysis of Bistable Piezoelectric Energy Harvester with a New-Type Dynamic Amplifier. Computational Intelligence and Neuroscience. 2022;2022:7155628.

[68] Kuang Y, Yang Z, Zhu M. Design and characterisation of a piezoelectric knee-joint energy harvester with frequency up-conversion through magnetic plucking. Smart Materials and Structures. 2016;25(8):085029.

[69] Wang J-X, Su W-B, Li J-C, Wang C-M. A rotational piezoelectric energy harvester based on trapezoid beam: Simulation and experiment. Renewable Energy. 2022;184:619-26.

[70] Tang H, Hua C, Huang H, Liu W, Yang Z, Yuan Y, et al. Low-frequency vibration energy harvesting: a comprehensive review of frequency up-conversion approaches. Smart Materials and Structures. 2022;31(10):103001.

[71] Haertling GH. Ferroelectric Ceramics: History and Technology. Journal of the American Ceramic Society. 1999;82(4):797-818.

[72] Mossi KM, Selby GV, Bryant RG. Thin-layer composite unimorph ferroelectric driver and sensor properties. Materials Letters. 1998;35(1):39-49.

[73] Pourashraf T, Bonello P, Truong J. Analytical and Experimental Investigation of a Curved Piezoelectric Energy Harvester. Sensors [Internet]. 2022; 22(6).

[74] Gao F, Liu G, Fu X, Li L, Liao WH. Lightweight Piezoelectric Bending Beam-Based Energy Harvester for Capturing Energy From Human Knee Motion. IEEE/ASME Transactions on Mechatronics. 2022;27(3):1256-66.

[75] Umeda M, Nakamura K, Ueha S. Analysis of the transformation of mechanical impact energy to electric energy using piezoelectric vibrator. Japanese Journal of Applied Physics. 1996;35(5S):3267.

[76] Kim S, Clark WW, Wang Q-M. Piezoelectric Energy Harvesting with a Clamped Circular Plate: Experimental Study. Journal of Intelligent Material Systems and Structures. 2005;16(10):855-63.

[77] Shixin YL, Li Q. DESIGN AND STUDY OF A MOONIE PZT MICROACTUATOR SLIDER DRIVEN DEVICE FOR HARD DISK DRIVES. ITE Technical Report. 2001;25.69:81-6.

[78] Kim H, Tadesse Y, Priya S. Piezoelectric Energy Harvesting. In: Priya S, Inman DJ, editors. Energy Harvesting Technologies. Boston, MA: Springer US; 2009. p. 3-39.

[79] Bejarano F, Feeney A, Lucas M. A cymbal transducer for power ultrasonics applications. Sensors and Actuators A: Physical. 2014;210:182-9.

[80] Jasim A, Wang H, Yesner G, Safari A, Maher A. Optimized design of layered bridge transducer for piezoelectric energy harvesting from roadway. Energy. 2017;141:1133-45.

[81] Wu L, Chure M-C, Wu K-K, Tung C-C. Voltage Generated Characteristics of Piezoelectric Ceramics Cymbal Transducer. Journal of Materials Science and Chemical Engineering. 2014;02:32-7.

[82] Liu X, Wang J. Performance Exploration of A Radially Layered Cymbal Piezoelectric Energy Harvester under Road Traffic Induced Low Frequency Vibration. IOP Conference Series: Materials Science and Engineering. 2019;542:012075.

[83] Zhao H, Ling J, Fu P. A Review of Harvesting Green Energy from Road. Advanced Materials Research. 2013;723:559-66.

[84] Moure A, Izquierdo Rodríguez MA, Rueda SH, Gonzalo A, Rubio-Marcos F, Cuadros DU, et al. Feasible integration in asphalt of piezoelectric cymbals for vibration energy harvesting. Energy Conversion and Management. 2016;112:246-53.

[85] Yuan J-b, Shan X-b, Xie T, Chen W-s. Energy harvesting with a slotted-cymbal transducer. Journal of Zhejiang University-SCIENCE A. 2009;10(8):1187-90.

[86] Yuan J, Shan X, Xie T, Chen W. Modeling and Improvement of a Cymbal Transducer in Energy Harvesting. Journal of Intelligent Material Systems and Structures - J INTEL MAT SYST STRUCT. 2010;21:765-71.

[87] Long SX, Khoo SY, Ong ZC, Soong MF, editors. Finite element analysis of a dual-layer substrate sandwiched bridge piezoelectric transducer for harvesting energy from asphalt pavement. 2019 IEEE International Conference on Sensors and Nanotechnology; 2019 24-25 July 2019.

[88] Mo C, Arnold D, Kinsel WC, Clark WW. Modeling and experimental validation of unimorph piezoelectric cymbal design in energy harvesting. Journal of Intelligent Material Systems and Structures. 2013;24(7):828-36.

[89] Arnold D, Kinsel W, Clark W, Mo C. Exploration of New Cymbal Design in Energy Harvesting. Proceedings of SPIE - The International Society for Optical Engineering. 2011;7977.

[90] Daniels A, Zhu M, Tiwari A. Design, analysis and testing of a piezoelectric flex transducer for harvesting bio-kinetic energy. Journal of Physics Conference Series. 2013;476:2047.

[91] Luo L, Liu D, Zhu M, Ye J. Metamodel-assisted design optimization of piezoelectric flex transducer for maximal bio-kinetic energy conversion. Journal of Intelligent Material Systems and Structures. 2017;28(18):2528-38.

[92] Li X, Guo M, Dong S. A Flex-Compressive-Mode Piezoelectric Transducer for Mechanical Vibration/Strain Energy Harvesting. IEEE transactions on ultrasonics, ferroelectrics, and frequency control. 2011;58:698-703.

[93] Zhao H, Qin L, Ling J. Test and Analysis of Bridge Transducers for Harvesting Energy from Asphalt Pavement. International Journal of Transportation Science and Technology. 2015;4(1):17-28.

[94] Zhao H, Qin L, Ling J. Synergistic performance of piezoelectric transducers and asphalt pavement. International Journal of Pavement Research and Technology. 2018;11(4):381-7.

[95] Palosaari J, Leinonen M, Hannu J, Juuti J, Jantunen H. Energy harvesting with a cymbal type piezoelectric transducer from low frequency compression. Journal of Electroceramics. 2012;28(4):214-9.

[96] Leinonen M, Palosaari J, Juuti J, Jantunen H. Combined electrical and electromechanical simulations of a piezoelectric cymbal harvester for energy harvesting from walking. Journal of Intelligent Material Systems and Structures. 2013;25(4):391-400.

[97] Dutoit NE, Wardle BL, Kim S-G. DESIGN CONSIDERATIONS FOR MEMS-SCALE PIEZOELECTRIC MECHANICAL VIBRATION ENERGY HARVESTERS. Integrated Ferroelectrics. 2005;71(1):121-60.

[98] Xu C, Ren B, Di W, Liang Z, Jiao J, Li L, et al. Cantilever driving low frequency piezoelectric energy harvester using single crystal material 0.71Pb(Mg1/3Nb2/3)O3-0.29PbTiO3. Applied Physics Letters. 2012;101(3):033502.

[99] Xu C, Ren B, Liang Z, Chen J, Zhang H, Yue Q, et al. Nonlinear output properties of cantilever driving low frequency piezoelectric energy harvester. Applied Physics Letters. 2012;101(22):223503.

[100] Tufekcioglu E, Dogan A. A flextensional piezo-composite structure for energy harvesting applications. Sensors and Actuators A: Physical. 2014;216:355-63.

[101] Zou H-X, Zhang W-M, Wei K-X, Li W-B, Peng Z-K, Meng G. A Compressive-Mode Wideband Vibration Energy Harvester Using a Combination of Bistable and Flextensional Mechanisms. Journal of Applied Mechanics. 2016;83(12).

[102] Zou H-X, Zhang W, Li W-B, Hu K-M, Wei K-x, Peng Z, et al. A broadband compressive-mode vibration energy harvester enhanced by magnetic force intervention approach2017. 163904 p.

[103] Yang Z, Zu J, Luo J, Peng Y. Modeling and parametric study of a force-amplified compressive-mode piezoelectric energy harvester. Journal of Intelligent Material Systems and Structures. 2016;28(3):357-66.

[104] Yang Z, Zhu Y, Zu J. Theoretical and experimental investigation of a nonlinear compressive-mode energy harvester with high power output under weak excitations. Smart Materials and Structures. 2015;24:025028.

[105] Purviance T, Wickler S, Clayson K, Barnes T, Mo C, editors. Development of low-profile piezoelectric energy harvester for high load application. 2013 1st IEEE Conference on Technologies for Sustainability (SusTech); 2013: IEEE.

[106] Wang X, Shi Z, Wang J, Xiang H. A stack-based flex-compressive piezoelectric energy harvesting cell for large quasi-static loads. Smart Materials and Structures. 2016;25(5):055005.

[107] Wang X, Shi Z. Double piezoelectric energy harvesting cell: modeling and experimental verification. Smart Materials and Structures. 2017;26(6):065002.

[108] Li Z, Zu J, Yang Z. Introducing hinge mechanisms to one compressive-mode piezoelectric energy harvester. Journal of Renewable and Sustainable Energy. 2018;10(3):034704.

[109] Wang Y, Yang Z, Cao D. On the offset distance of rotational piezoelectric energy harvesters. Energy. 2021;220:119676.

[110] Ma H-W, Yao S-M, Wang L-Q, Zhong Z. Analysis of the displacement amplification ratio of bridge-type flexure hinge. Sensors and Actuators A: Physical. 2006;132(2):730-6.

[111] Shao SB, Xu ML, Chen J, Feng B. Optimal design of the large stroke piezoelectric actuator using rhombic mechanism. 2014.

[112] Ling M, Cao J, Zeng M, Lin J, Inman DJ. Enhanced mathematical modeling of the displacement amplification ratio for piezoelectric compliant mechanisms. Smart Materials and Structures. 2016;25(7):075022.

[113] Zhou H, Henson B. Analysis of a diamond-shaped mechanical amplifier for a piezo actuator2007. 1-7 p.

[114] Ouyang P, Zhang W, Gupta M. Design of a New Compliant Mechanical Amplifier2005.

[115] Wen S, Xu Q, Zi B. Design of a New Piezoelectric Energy Harvester Based on Compound Two-Stage Force Amplification Frame. IEEE Sensors Journal. 2018;18(10):3989-4000.

[116] Feenstra J, Granstrom J, Sodano H. Energy harvesting through a backpack employing a mechanically amplified piezoelectric stack. Mechanical Systems and Signal Processing. 2008;22(3):721-34.

[117] Sosnicki O, Lhermet N, Claeyssen F. Vibration energy harvesting in aircraft using piezoelectric actuators. 10th international conference on new actuators; 14-16 June 2006; Bremen, Germany2006. p. 968-71.

[118] Zhou W, Zuo L. A Novel Piezoelectric Multilayer Stack Energy Harvester With Force Amplification2013.

[119] CEDRAT TECHNOLOGIES. Amplified Piezo Actuators 2020 [Available from: https://www.cedrat-technologies.com/en/products/actuators/amplified-piezo-actuators.html.

[120] Lee HJ, Sherrit S, Tosi LP, Walkemeyer P, Colonius T. Piezoelectric Energy Harvesting in Internal Fluid Flow. Sensors. 2015;15(10).

[121] Liu W, Badel A, Formosa F, Wu Y, Agbossou A. Novel piezoelectric bistable oscillator architecture for wideband vibration energy harvesting2013. 035013 p.

[122] Liu W, Badel A, Formosa F, Wu Y, Agbossou A. Wideband energy harvesting using the combination of optimized synchronous electric charge extraction circuit and bistable harvester2013. 5038 p.

[123] Bencheikh N, Pagès A, Forissier T, Porchez T, Kras A, Badel A, et al., editors. A bistable piezoelectric harvester for wideband mechanical frequency excitation. 14th International Conference on New Actuators; 2014 23e25 June; Bremen, Germany.

[124] Li Z, Peng X, Hu G, Zhang D, Xu Z, Peng Y, et al. Towards real-time self-powered sensing with ample redundant charges by a piezostack-based frequency-converted generator from human motions. Energy Conversion and Management. 2022;258:115466.

[125] Xu T-B, Jiang, X.,Su, J.,Rehrig, P.W.,Hackenberger, W.S.,, inventorHybrid piezoelectric energy harvesting transducer system. US patent 7,446,459 B2. 2008.

[126] Tolliver L, Xu T-B, Jiang X. Finite element analysis of the piezoelectric stacked-HYBATS transducer. Smart Materials and Structures. 2013;22(3):035015.

[127] Xu T-B, Jiang X, Su J. A piezoelectric multilayer-stacked hybrid actuation/transduction system. Applied Physics Letters. 2011;98(24):243503.

[128] Mottard P, St-Amant Y. Analysis of flexural hinge orientation for amplified piezo-driven actuators. Smart Materials and Structures. 2009;18:035005.

[129] Xu Q, Li Y. Analytical modeling, optimization and testing of a compound bridge-type compliant displacement amplifier. Mechanism and Machine Theory. 2011;46(2):183-200.

[130] Qi K-Q, Xiang Y, Fang C, Zhang Y, Yu C-s. Analysis of the displacement amplification ratio of bridge-type mechanism. Mechanism and Machine Theory. 2015;87.

[131] Choi K-B, Lee JJ, Kim GH, Lim HJ, Kwon SG. Amplification ratio analysis of a bridge-type mechanical amplification mechanism based on a fully compliant model. Mechanism and Machine Theory. 2018;121:355-72.

[132] Lee Y-L, Barkey ME. Chapter 4 - Stress-Based Uniaxial Fatigue Analysis. In: Lee Y-L, Barkey ME, Kang H-T, editors. Metal Fatigue Analysis Handbook. Boston: Butterworth-Heinemann; 2012. p. 115-60.

[133] Wang Y, Chen W, Guzman P. Piezoelectric stack energy harvesting with a force amplification frame: Modeling and experiment. Journal of Intelligent Material Systems and Structures. 2016;27(17):2324-32.

[134] Zhang J, Yu X, Zhao W, Qu D. A piezoelectric vibration energy harvester based on the reverse-rhombus double-bridge force amplification frame. Journal of Physics D: Applied Physics. 2021;54(36):365501.

[135] Long SX, Khoo SY, Ong ZC, Soong MF. Design, modeling and testing of a new compressive amplifier structure for piezoelectric harvester. Smart Materials and Structures. 2021;30(12):125010.

[136] Evans M, Tang L, Tao K, Aw K. Design and optimisation of an underfloor energy harvesting system. Sensors and Actuators A: Physical. 2019;285:613-22.

[137] Chen WS, Wang Y, Deng W. Deformable force amplification frame promoting piezoelectric stack energy harvesting: Parametric model, experiments and energy analysis. Journal of Intelligent Material Systems and Structures. 2017;28(7):827-36.

[138] Liu H, Hua R, Lu Y, Wang Y, Salman E, Liang J. Boosting the efficiency of a footstep piezoelectric-stack energy harvester using the synchronized switch technology. Journal of Intelligent Material Systems and Structures. 2019;30(6):813-22.

[139] Evans M, Tang LH, Aw KC. Modelling and optimisation of a force amplification energy harvester. Journal of Intelligent Material Systems and Structures. 2018;29(9):1941-52.

[140] Qian F, Xu TB, Zuo L. Design, optimization, modeling and testing of a piezoelectric footwear energy harvester. Energy Conversion and Management. 2018;171:1352-64.

[141] Kuang Y, Chew ZJ, Zhu M. Strongly coupled piezoelectric energy harvesters: Finite element modelling and experimental validation. Energy Conversion and Management. 2020;213:112855.

[142] Tolliver L, Jiang X, Xu T-B. Piezoelectric Actuators With Active and Passive Frames2013.

[143] Xu TB, editor Piezoelectric Transducer Inventions in the Last Two Decades. OCEANS 2022, Hampton Roads; 2022 17-20 Oct. 2022.

[144] Wen S, Xu Q, editors. Design of a two-stage force amplification frame for piezoelectric energy harvesting. 2017 IEEE International Conference on Cybernetics and Intelligent Systems (CIS) and IEEE Conference on Robotics, Automation and Mechatronics (RAM); 2017 19-21 Nov. 2017.

[145] Wang L, Chen S, Zhou W, Xu T-B, Zuo L. Piezoelectric vibration energy harvester with two-stage force amplification. Journal of Intelligent Material Systems and Structures. 2016;28(9):1175-87.

[146] Qian F, Xu T-B, Zuo L. Piezoelectric energy harvesting from human walking using a two-stage amplification mechanism. Energy. 2019;189:116140.

[147] Wen S, Xu Q. Design of a Novel Piezoelectric Energy Harvester Based on Integrated Multistage Force Amplification Frame. IEEE/ASME Transactions on Mechatronics. 2019;24(3):1228-37.

[148] Duan X, Cao D, Li X, Shen Y. Design and dynamic analysis of integrated architecture for vibration energy harvesting including piezoelectric frame and mechanical amplifier. Applied Mathematics and Mechanics. 2021;42(6):755-70.

[149] Wu Z, Xu Q. Design and testing of a novel bidirectional energy harvester with single piezoelectric stack. Mechanical Systems and Signal Processing. 2019;122:139-51.

[150] Siddique ARM, Mahmud S, Heyst BV. A comprehensive review on vibration based micro power generators using electromagnetic and piezoelectric transducer mechanisms. Energy Conversion and Management. 2015;106:728-47.

[151] Shenck NS, Paradiso JA. Energy scavenging with shoe-mounted piezoelectrics. IEEE Micro. 2001;21(3):30-42.

[152] Ren B, Or SW, Zhao X, Luo H. Energy harvesting using a modified rectangular cymbal transducer based on 0.71Pb(Mg1/3Nb2/3)O3–0.29PbTiO3 single crystal. Journal of Applied Physics. 2010;107(3):034501.

[153] Wei H, Shirinzadeh B, Li W, Clark L, Pinskier J, Wang Y. Development of Piezo-Driven Compliant Bridge Mechanisms: General Analytical Equations and Optimization of Displacement Amplification2017. 238 p.

(Word count: 17076 words)